Supersonic Mixing Enhancement by Vorticity for High-Speed Propulsion

Final Report
for the Period April 1, 1988 - June 30, 1991

Submitted to:

Dr. G. B. Northam, MS-168
NASA-Langley Research Center
Hampton, VA 23665-5225

Submitted by:

Dr. Gary S. Settles
Professor of Mechanical Engineering
Director, Gas Dynamics Laboratory

October 1991

PENNSTATE GAS DYNAMICS LABORATORY

ABSTRACT

This report discusses the results of a three year study on vortex enhancement of supersonic mixing supported under grant NAG-1-872. Recent interest in compressible mixing has spurred research in the field of high speed shear layers. It has been established that shear layer growth diminishes with increasing convective Mach number; this Mach number is the relative mach number of the large scale structures in the shear layer with respect to the Mach numbers on either side of the shear layer. Efforts to enhance shear layer growth rates at high convective Mach number have proven unsuccessful. This research project was started to evaluate the effect of swirl on compressible mixing rates. Previous analytical and experimental results seem to indicate that swirling flow may significantly modify the shear layer, in some cases resulting in enhanced mixing. Previous studies of the effect of swirl on compressible mixing were incomplete since the amount of swirl in the flowfield was not quantified. This study was undertaken to conclusively determine the effect of swirl on supersonic mixing, including the quantification of the swirl. Preliminary results indicate that the swirl modestly enhances the mixing rates.

NOMENCLATURE

Variables:

a - acoustic speed, constants
A - area
D - diameter
f - frequency
L - distance downstream
M - Mach number
n - azimuthal wave number
R - velocity ratio
Re - Reynolds number
S - density Ratio
St - Stokes or Strouhal number
T - temperature
u - velocity
α - axial wave number
γ - ratio of specific heats
ρ - density
μ - kinematic viscosity
ν - dynamic viscosity
δ - shear layer thickness
θ - vane angle, non-dimensional temperature
τ - characteristic period

Subscripts:

a - ambient
c - convective
crit - critical
f - fluid
i - injector, intensity level, inner
inc - incompressible
j - jet
o - stagnation, outer
p - particle
r - recovery
t - tunnel
v - vortex
x,y,z - cartesian coordinates

1 INTRODUCTION

In recent years a great deal of effort has been spent on trying to understand the fundamental physics of high speed shear layers. Lately, this topic has become a priority area of study due to the NASP (National Aerospace Plane) project. This interest in high speed shear layers was due to the necessity of mixing fuel and air in a SCRAMJET engine of such a vehicle. Since the velocities in the combustion chamber of a SCRAMJET are supersonic, rapid mixing of the fuel and air is necessary. However, it was known at the outset that the mixing rates for two streams, with a given velocity and density ratio, decreased with increasing Mach number. Therefore, several studies were undertaken to attempt to understand and increase the rates of combustion in supersonic flows. Northam and Anderson[1] (1986) discuss such research ongoing at NASA-LaRC. These studies include both experimental[2] and computational[3] efforts. However, fundamental research on non-reacting mixing layers is needed to complement the combustion research. This research is necessary so that the controlling mechanisms of the high speed shear layer and shear layer mixing may be studied without the complicating presence of combustion.

More recently, the High Speed Civil Transport (HSCT) program has identified several critical technology needs, many of which are related to high-speed shear layers. These needs are summarized by Seiner and Kresja[4]. One area was the issue of jet engine noise associated with takeoff and landing. A method of lowering takeoff noise is through the use of ejector nozzles which also have the beneficial effect of increased thrust. An important parameter associated with ejector nozzles is the so-called augmentation, a measure of the entrainment of the secondary stream by the primary stream (see Figure 1). The entrainment of the secondary stream is important in that

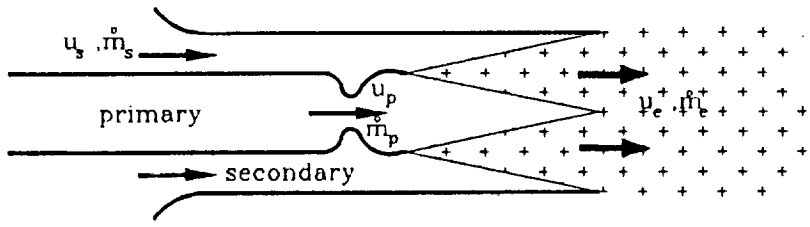

Figure 1 - Schematic of Ejector Nozzle

it dictates the amount of mass entrained as well as the induced velocity given to the secondary stream by the primary stream. A controlling factor of this augmentation ratio is how fast the primary and secondary streams can be mixed. Thus, the HSCT project also provides a practical application for compressible mixing enhancement techniques.

The study of compressible turbulent vortices is valuable since it may contribute to the understanding of complex turbulent flows. Studying the mixing properties of vortical flows in order to more fully the appreciate the underlying physics of compressible turbulent shear layers is of value in itself; any direct application of the results, such as those listed above, is fortunate.

This study focuses on the use of swirl to enhance the compressible mixing process. The use of swirl to increase mixing has been suggested by many researchers. Swithenbank and Chigier[5] (1969) proposed to enhance supersonic mixing with swirl based on observations in subsonic and transonic flows. Instability analysis by several researchers including Lessen *et al*[6](1974) has suggested that swirl may destabilize otherwise stable flowfields. Recently, Kumar *et al*[7] (1987) reviewed techniques for enhancing mixing. Among these techniques were: provision of increased mixing area, control of vorticity production, imposition of swirl or longitudinal vortex motion, design of combustor ensuring turbulence augmentation, and shock interactions. The current study addresses all these issues through the study of the mixing process of a supersonic vortex. This study encompasses several fundamental fields of study including compressible shear layers, swirling flowfields, and vortex breakdown. Both experimental and analytical research in each of these fields is discussed in the literature review.

This thesis proposal is organized in the following manner. The existing literature is reviewed and the problem statement described in the first section. The second section discusses the test facilities and hardware. Instrumentation and experimental methods are described in detail in that section. The third section describes the reduction processes for the data taken, and fourth section presents the results to date. The final section presents the conclusions to date and the steps required to complete this project.

2 LITERATURE SURVEY AND PROBLEM STATEMENT

As stated above, supersonic mixing enhancement by means of streamwise vorticity has several related fields of interest. Some background in these fields is necessary to completely understand the present problem and experimental approach.

2.1 Compressible Turbulent Shear Layers

2.1.1 Planar Shear Layers

The importance of compressibility in shear layers has been known for a long time. The reduction of mixing rates in compressible shear layers was observed early on, but only recently have the reasons for this reduction been explored. Dimotakis[8] (1989) has summarized much of the

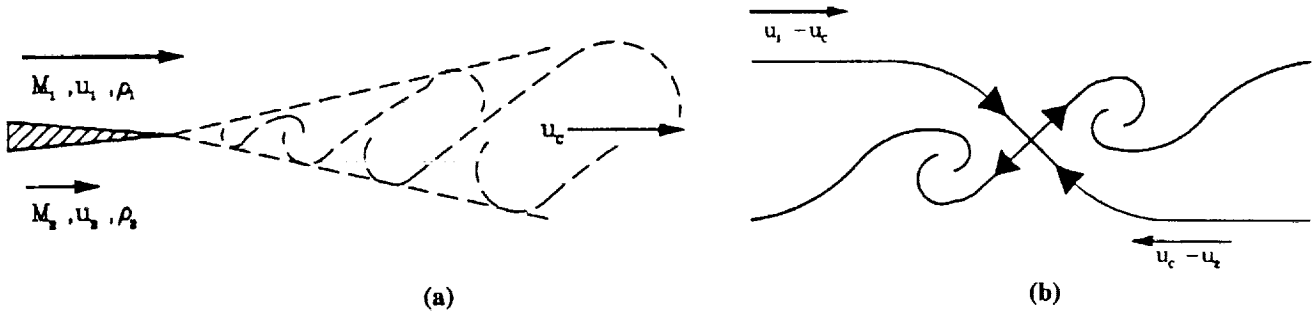

Figure 2 -The planar shear layer (a) in the laboratory frame of reference and (b) in the convective frame of reference

current understanding of shear layers. One theory attributes the reduction in mixing of the compressible shear layer to the density ratio between the two streams. In subsonic flows the mixing rate of two streams was already known to be a function of the velocity ratio of the two streams. However, the role of the density ratio was not well understood before Brown and Roshko[9] studied the effect of density ratio on incompressible turbulent mixing rates. In their landmark study, they found that the mixing rate was a function of the density ratio of the two streams. However, the 30 % reduction in vorticity thickness for a density ratio of 7 in subsonic shear layers does not account for the drastic reduction of 300% seen in a compressible shear layer of the same density ratio. Therefore, they attributed the major portion of this effect to compressibility alone. In addition, their flow visualization experiments revealed large scale structure that dominated the mixing layer.

Following the work of Bogdanoff[10](1983), Papamoschou and Roshko[11](1988) transformed the coordinate frame from a laboratory frame of reference, Figure 2a, to a frame of reference convecting with the large scale structures, Figure 2b. They reasoned that the saddle point in the convective frame of reference requires that the total pressure of the two streams be equal. They called the Mach number in this frame of reference the convective Mach number (M_c). The normalized spreading rates (δ'/δ'_{inc}) collapse to a common curve when plotted versus M_c as shown in Figure 3. The normalized spreading rate drops quickly with increasing M_c, but asymptotes to

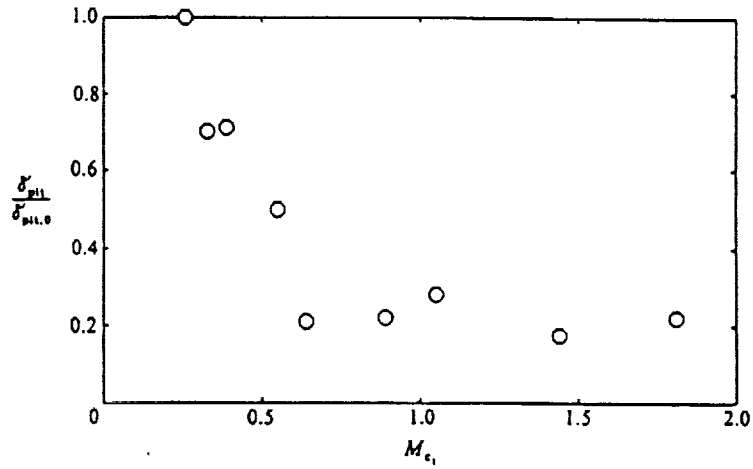

Figure 3 - Normalized shear layer growth rate versus convective Mach Number (from Papamoschou and Roshko[11](1988))

about 0.2 at a convective Mach number somewhat less than unity. They pointed out that no shocks or expansions are believed to exist in the convective frame of reference for $M_c < 1$; thus, the decrease in mixing must be due to some other phenomena. They postulated that energy was radiated away from the shear layer rather than being used for growth. The asymptotic nature of the curve in Figure 2 was attributed to a diminishing but ever present subsonic sub-layer in the convective frame of reference. An additional comment was made that oblique structures would have an "effective" convective Mach number that depended on the angle of the structure with respect to the freestream direction. If turbulent structures became oblique as M_c increased, the effectively-reduced convective Mach number and growth rate associated with it could account for the asymptotic nature of the mixing curve at high M_c.

Since these original studies, a significant amount of additional research has gone into understanding compressible shear layers. Papamoschou[12] observed that structures on opposite sides of the shear layer moved at different speeds, and these speeds did not agree with the convective Mach number predicted by Figure 3. Turbulence levels in the compressible shear layer have also been studied[13,14,15,16]. A significant reduction in turbulence with increasing M_c was found by all researchers, while Goebel & Dutton[14](1990) found that the turbulence anisotropy increased with M_c. Elliot *et al*[15](1990) performed one- and two-point correlations with pressure probes. Although the intrusiveness of the probes makes the results somewhat suspect, they showed the frequency content of the shear layer to be between 4 and 15 kHz. In addition, they found that the streamwise space-time correlations calculation of M_c agreed well with Figure 3. However, spanwise correlations were very low, suggesting a highly three-dimensional shear layer.

This highly 3-D structure of 2-D compressible shear layers has been confirmed visually by Clemens *et al*[17,18](1990). For one value of M_c (0.6) they saw large-scale structures when performing streamwise cuts of the shear layer with a laser sheet. However, when they cut spanwise these structures did not persist across the shear layer. Further study at various values of M_c revealed a transition from 2-D to 3-D structure with increasing convective Mach number.

One reason for carrying out fundamental studies of the shear layer was to increase the understanding of the underlying physics so that intelligent methods of enhancing supersonic mixing could be attempted. Papamoschou[19] added obliquity to the flow in an attempt to reduces the effective M_c. The several methods used to create this obliquity proved to be ineffective. Dolling *et al*[20] (1990) attempted to add streamwise vorticity to the shear layer by installing vortex generators on the trailing edge of the splitter plate. These vortex generators showed only a modest increase of 30% in growth rate over the case without the generators. Dolling *et al*[21] studied the effect of a shock wave on the growth rate of the shear layer. They passed a shock wave across the boundary layer upstream of the splitter plate lip and across the shear layer downstream. In both cases they

noticed no increase in mixing rate except locally. Clemens and Mungal[22](1990) introduced streamwise vorticity to a 2-D shear layer by means of perturbing the boundary layer leaving the splitter plate. Both a delta wing and an oblique shock were used to generate longitudinal vorticity. Although no quantitative measurements were made, laser sheet images showed an increase of boundary area between the two streams.

2.1.2 Axisymmetric Shear Layers

Basic Studies on axisymmetric shear layers have also been performed.[23] These investigations reached conclusions similar to their two-dimensional counterparts. Although the flows are fundamentally different, there appear to be many similarities at least in the developing regions. The planar spreading-rate trend with M_c appears to hold for axisymmetric jets also. Fourgette and Dibble[24](1990) found deviations of structure velocities from theoretically-predicted rates as did McIntyre and Settles[25](1991). McIntyre and Settles also found a frequency spectrum similar to that of 2-D results, with most of the energy in the lower frequencies, although the spectrum appears more broadband. They also observed that energy moved to the lower frequencies the farther downstream the measurements were made. In addition, two-point measurements revealed no constant spacing of the structures. However, the existence of large scale structures in the flowfield appeared to be supported by the concentration measurements of Fourgette *et al*[26] (1991). The large departure from the average concentration at a given point in the shear layer seemed to suggest some large scale structure. Instantaneous laser sheet pictures in the present study also seem to support the existence of large scale structure. Figure 4 shows several cross-sectional views of the same jet at different points in time. The images show large differences in appearance suggesting that large convecting structures were present.

Two unique enhancement studies on axisymmetric shear layers were performed by Lepicovsky *et al*[27](1987) and Samimy *et al*[28](1991). Lepicovsky observed the shear layer of fully-expanded supersonic jets under acoustic excitation of 120 dB. In varying the frequency, they observed large coherent structures in the shear layer at certain excitation frequencies. The most amplified structures were observed at a Strouhal number, $St = (f^* D_j / U_j)$, of 0.4. Such regularly-spaced large-scale structures have not been found in unexcited compressible flows. Samimy *et al* placed tabs at the exit of the nozzle to induce streamwise vorticity. With the proper configuration, the jet bifurcated increasing the surface area of the jet significantly. This unique process in jets is not possible in a two-dimensional shear layer.

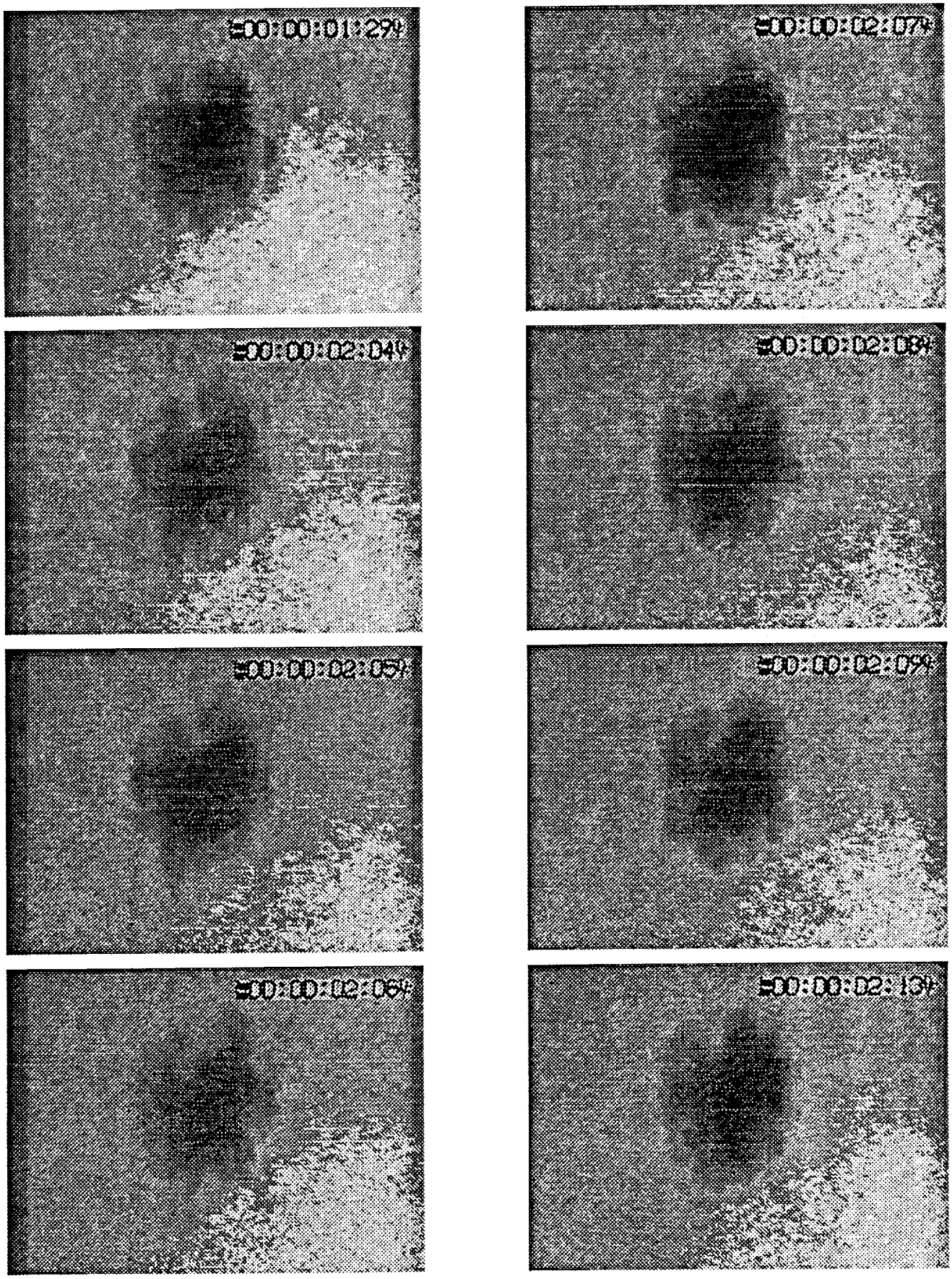

Figure 4 Instantaneouslight sheet images of Mach 2.95 helium jet.

2.1.3 Instability Analysis of Compressible Shear Layers

Analysis of compressible turbulent shear layers is difficult at best and impossible in many cases. One form of analysis that sheds light on the physics occurring within compressible shear layers is instability analysis. Such studies have been able to predict with some accuracy certain features of the flow. With this in mind, other interesting results of the studies lend experimentalists a guide for planning their experiments.

Tam and Hu[29](1988) found three families of instability waves in an axisymmetric jet in agreement with previous experimental work. These wave families were called the Kelvin-Helmholtz (K-H), subsonic, and supersonic instabilities. Kelvin-Helmholtz instabilities are the instabilities that cause 2-D structures in low speed flows. Tam and Hu found that K-H instabilities have their maximum growth rate at low speeds. Subsonic waves were found to exist only within the jet and decayed rapidly outside the jet; thus, their effect on growth rates was insignificant. Supersonic instabilities were only found when the jet velocity was greater than the sum of the acoustic velocities of the jet and the surrounding environment, $u_j > (a_a + a_j)$. For each azimuthal wave number there is a family of instability waves with different radial wave numbers. The growth rate of these waves increases with increasing Mach number and becomes dominant at some Mach number M_{crit}. The Strouhal number of the most unstable modes was found to be in the range of 0.25 to 0.55, comparing favorably with the results of Lepicovsky et. al.[27] (1987).

An analytical study to determine growth rates for different modes was performed by Morris *et al*[30](1990). In this study they showed that the axisymmetric and helical growth rates were different with the helical mode dominating in certain cases. In concurrence with experimental findings, they showed that the growth rates for both axisymmetric and 2-D shear layers reduces with M_c. In addition, for the specific conditions of the 2-D shear layer modeled, they found that the most unstable wave propogated with an angle of 55 degrees.

These models have accurately predicted some features of compressible shear layers such as the decrease in growth rates with M_c. With this in mind, the results suggest exciting the helical modes that are predicted to have the greatest growth rate at supersonic Mach numbers. If these unstable modes were excited, the shear layer growth could be enhanced significantly.

2.2 VORTEX ENHANCEMENT OF MIXING

2.2.1 Low Speed Results

2.2.1.1 Experimental Studies

Vortical flowfields have long been utilized in subsonic combustion. An overview of the use of vortices in practical applications is given by Escudier[31](1987). Many researchers, including Chigier and Chervinsky[32](1967), Delery *et al*[33] (1984), have studied swirling flowfields in detail for the purpose of explaining observed phenomena. The results of these studies and efforts to explain the process of vortex breakdown, discussed later in this section, have resulted in the following conclusions. First, swirling motions create pressure gradients within the flowfield that in case of mild to stong swirl cause an axial velocity deficit on the axis. In addition, jet width and rate of entrainment increase with swirl. Finally, if the swirl is increased sufficiently or a significant pressure gradient is encountered, the vortex will burst. Due to these factors, and results from transonic flows, Swithenbank and Chigier[5] suggested that similar phenomena may occur in supersonic vortical flows.

2.2.1.2 Instability Analysis

In addition to experimental work, instability analyses of several flowfields with swirl suggest that the addition of an azimuthal component may be destabilizing. Lessen *et al*[34](1974) studied the addition of swirl to a wake flow. (Note that this flow is not dissimilar to the experimental flows discussed above in that the experimental flows often show a wake-like core in the flowfields studied.) Their inviscid study of the swirling flow showed that all positive azimuthal modes were stabilized by adding swirl. On the opposite side, the negative azimuthal modes were destabilized for small amounts of swirl and stabilized for large amounts of swirl. In addition, for a given amount of swirl, the higher the negative azimuthal mode was, the greater the instability (up to n=6).

Later studies by Lessen and Paillet[35](1974) and Leibovitch and Stewartson[36](1983) extended this work. The former study added viscosity to their model and confirmed the inviscid studies results. In addition they determined a critical Reynold number for each azimuthal mode and found these were quite low. This suggests that, at normal Reynold numbers, the transition from a stable to an unstable condition would be a "sharp function" of the degree of swirl. They also determined that the swirl at which the azimuthal modes would become stable again was greater the higher the mode. Leibovitch and Stewartson repeated the inviscid study of Lessen *et al*[34] and concurred with its results. In addition, they performed an asymptotic analysis to determine if the

maximum amplification rate was finite for large azimuthal wave numbers. The results of this analysis determined that a finite value of the growth rate existed as n approached infinity.

One experimental analysis that measured instabilities in a swirling flow was that of Singh and Uberoi[37](1976). They probed a laminar trailing vortex with X-wire-configured hot-wires and found two unstable modes n = 0 and n = + /-1. From their measurements they could not distinguish between positive and negative azimuthal modes. However, the helical mode was the more unstable of the two.

Obviously the theory and experiment discussed above do not apply directly to increasing mixing in compressible flows. However, they clearly show that a flow that is initially stable may be made unstable with the addition of swirl.

2.2.2 Supersonic Results

2.2.2.1 Experimental Results

Due to the preliminary evidence suggesting that compressible shear layers would mix faster in the presence of swirl, several studies were initiated. Povinelli and Ehlers[38](1972) investigated sonic parallel injection, with and without swirl, into a M = 2.7 air flow. Total temperature and concentration profiles were measured. These measurements indicated that there was little difference in the two flows. In a similar study, Schetz and Swanson[39](1973) studied coaxial injection into a M = 3.5 freestream. Cases with and without swirl were investigated with total temperature and total pressure surveys. As in the previous study, little difference was seen in flowfield structure. From the results of these studies, the researchers concluded that the addition of swirl did not enhance mixing. However, reexamining the total temperature results of both studies suggests that little swirl was actually present in the flowfield. In any case, the swirl was not quantified in either study, so the conclusion that swirl did not enhance mixing was somewhat premature.

Evidence that streamwise vorticity plays a large role in compressible mixing is shown by several studies. Swithenbank *et al*[40](1989) injected fuel in the vicinity of a delta wing vortex generator. They found a 30% increase in mixing efficiency over the baseline configuration. Tillman *et al*[41,42](1988,1989) investigated the flowfield near the exit of a mixer nozzle and found faster decay of centerline temperature and increased distribution of shear forces. These results were attributed to the inviscid stirring mechanism provided by large streamwise vortices in the flow. Driscoll[43](1986) showed comparable results while investigating supersonic mixer nozzles for chemical lasers. He found a similar increase of area where the injectant and ambient were in

contact. He termed this process "reactant surface stretching." Although these studies show that streamwise vorticity plays a role in supersonic mixing, none of them directly studied the mixing enhancement associated with swirling the entire injectant flow.

As a result of the inconclusiveness of preliminary studies of swirl enhancement of mixing, coupled with the promising results of enhanced mixing due to local streamwise vorticity, this study was initiated. A summary of the earliest results of this study[44] is included in the appendix. Briefly restated here, the addition of swirl to a Mach 3.0 air jet exiting into a Mach 3.5 freestream was

studied. The flowfield was analyzed both with probe surveys and laser light scattering visualization. For this low M_c flow, the addition of vorticity was seen to increase mass entrainment by 30%.

2.2.2.2 Analytical Results

Recently, Khorrami[45](1991) performed a temporal instability analysis of a compressible swirling jet. Although this study only considered cases with low degrees of swirl at relatively low Reynold number, it is the only study of its type. As in the incompressible analysis the growth rates of negative azimuthal modes were shown to increase significantly. Note that only azimuthal modes with n = +/-1 are unstable for jets without swirl. This analysis also showed that the growth-rate-damping effect of increasing M_c was still present, but less than in the case without swirl. This model leaves unanswered several questions:

Is there a swirl rate above which the flow stabilizes?
What is the swirl at which the growth rates are a maximum ?
Do azimuthal modes n<-2 asymptote to some to some finite growth rate as Re approaches infinity?

Although the studied flowfield is low Reynolds number and low swirl, the results seem to suggest that the swirling the compressible jet may delay or reduce the damping effect of compressibility on mixing.

Figure 5 - Spiral and Bubble forms of vortex breakdown. Taken from Sarpakaya[70].

2.2.3 Vortex Breakdown

2.2.3.1 Low Speed Results

The last related area of study is vortex breakdown. The phenomenon of vortex breakdown in incompressible flows has been studied in detail. Pictures of vortex breakdown are shown in Figure 5. This subject will be treated briefly here; further details may be found in excellent review articles by Hall[46](1972) and Leibovitch[47](1978).

Vortex breakdown occurs in flows with significant axial and tangential velocities. It only occurs in the presence of an adverse pressure along the axis of the vortex. This pressure gradient need not be in the exterior flow, as it can be self generated. If breakdown occurs, an increase in either the swirl or pressure gradient moves the location of breakdown upstream. Thus it is the combination of swirl and pressure gradient that determines if and where breakdown occurs.

There are three regions within the vortex breakdown flowfield: the approach flow region, the breakdown region and the wake region. The approach flow region is characterized by relatively small gradients and small fluctuations. The breakdown region contains a stagnation point on the axis with a region of reversed flow behind it. This region is characterized by large axial gradients. The wake region aft of the breakdown region contains a reorganized vortex with a wake-like axial velocity profile. There are also high turbulence levels within this region.

The exact cause of vortex breakdown is not well understood although it has been studied for many years. There are many theories that have attempted to predict when vortex breakdown occurs. The instability analyses discussed above have been used to explain breakdown. Another theory postulates that there is a critical state in vortex flows.[48] Vortex breakdown separates a region of supercritical flow, the approach flow, from a region of subcritical flow, the wake region. Hall[46] postulates that the upstream flow approaches the critical state, and when it is reached, vortex breakdown occurs. A third theory dictates that breakdown occurs when axial gradients become large.[46] A quasi-cylindrical flowfield is assumed for the approach flow with axial gradients which are small compared to radial gradients. When this quasi-cylindrical assumption fails due to large axial gradients, breakdown is assumed to occur. This theory lends itself to numerical solution in a manner similar to that of the prediction of boundary layer separation. A final theory postulates the build-up of waves near a critical point.[49] The success of these theories in predicting and understanding vortex breakdown is summed up by Fahler and Leibovitch[50](1977): "The embarrassing number of different theoretical notions has not, it must be admitted, led to a satisfactory understanding of the flows observed."

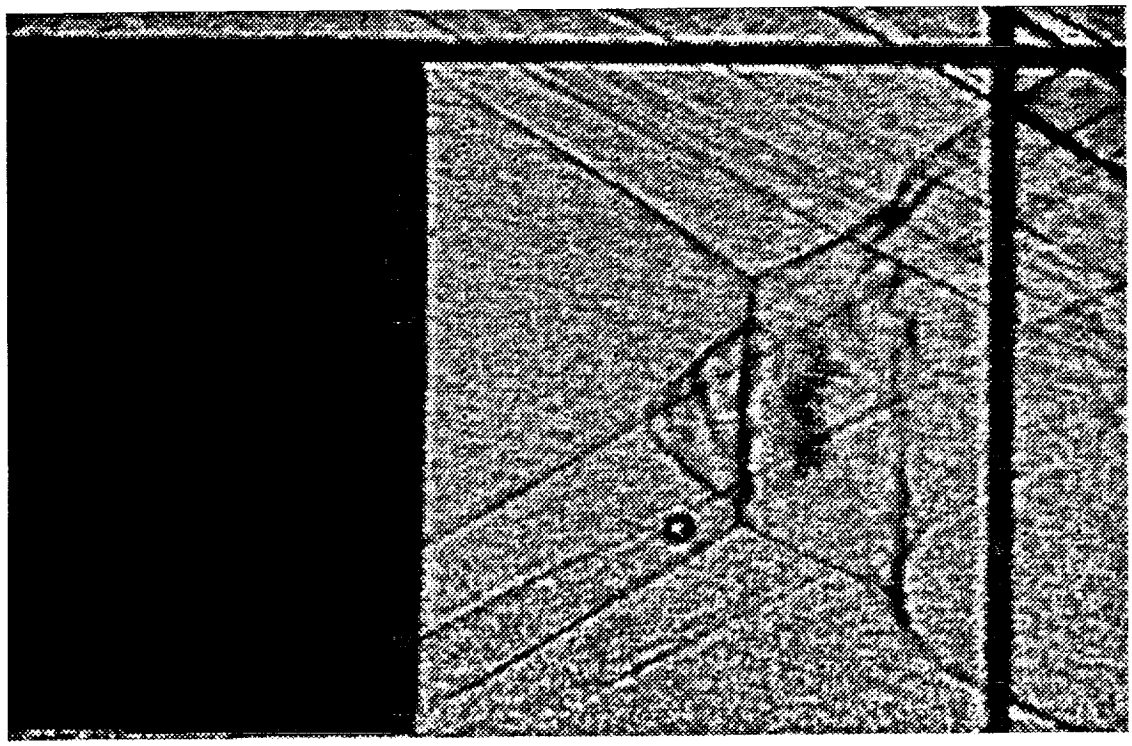

Figure 6 - Supersonic vortex breakdown in an underexpanded swirling jet. From Cattafesta and Settles[51].

Although the theory of vortex breakdown is not well developed, the characteristics of breakdown in subsonic flow are well established. If these same characteristics were present in supersonic vortex breakdown, they could be utilized to enhance compressible mixing.

2.2.3.2 High Speed Results

Vortex breakdown in supersonic flowfields has only recently been studied. Delery *et al*[53](1984) studied the interaction of a trailing vortex produced by a delta wing with a normal shock. Maximum tangential velocities up to 40% of the axial velocity were produced. They determined the limit of vortex breakdown over a range of Mach number as a function of swirl and normal shock strength (dictated by the Mach number). For one breakdown case, LDV surveys indicated a region of reversed flow. In this case the swirling motion decreased and dilated radially much like that of a dissipating vortex. The radius of the core doubled and turbulence intensities downstream significantly increased. Constant mass flow lines exhibit structure similar to the structure incompressible vortex breakdown.

Metwally[51](1990) and Metwally *et al* [52](1989) studied the addition of swirl to a highly overexpanded jet. A "bubble-shock" was observed where, in the no-swirl case, a simple Mach disc would have been located. This bubble-shock was highly unsteady and recompression shocks were noted downstream, suggesting a region of reversed flow. Cattafesta and Settles[53](1991) extended

this work comparing the overexpanded vortex case, Figure 6, with a streamwise vortex passing through a normal shock produced by a stalled inlet. Cutler and Levey[54](1991) used the mechanism of an overexpanded jet to study shock/vortex interaction in a free-jet facility. They noted that the mixing layer downstream of the shock/vortex interaction grew much faster than the case without swirl.

2.3 Summary

This literature survey has shown that there is promise in using swirl for enhancing compressible mixing. There is no single result which suggests that this enhancement technique may work. Rather, it is the sum of several results and suggestions across a broad range of research fields that leads one to conclude that vorticity may enhance mixing in the compressible range. Thus, this study is aimed at conclusively determining the role of swirl in compressible mixing.

2.4 PROBLEM STATEMENT

This study was undertaken to verify whether or not swirl enhances mixing over a large range of compressibility and swirl. In order to conclusively determine the effect of swirl, it has to be quantified for each case studied. The compressible mixing enhancement dependence on swirl, compressibility, and density ratio could then be determined from the results. With this information it was felt that future research would have the basic information needed to design experiments aimed at determining the mechanism behind swirl induced mixing enhancement.

3 TEST FACILITY AND HARDWARE

3.1 EXPERIMENTAL FACILITIES

3.1.1 Penn State Gas Dynamics Lab - Supersonic Wind Tunnel

The primary facility used for this study was the Penn State Supersonic Wind Tunnel pictured in Figure 7. This tunnel is an intermittent blow-down type with a Mach number range of 1.5 to 4.0. The Mach number is continuously variable by means of an asymmetric sliding block nozzle. The pressure reservoir has a volume of 57 cubic meters (2000 cu. ft.) and may be pressurized to 2 MPa (300 psi). The run time of the facility depends on the Mach number and total pressure and varies from 30 seconds to over 1 minute. The test section dimensions are 15.25 x 16.50 x 61.95 cm (6 x 6.5 x 24 in.) with visual access through both sidewalls and ceiling.

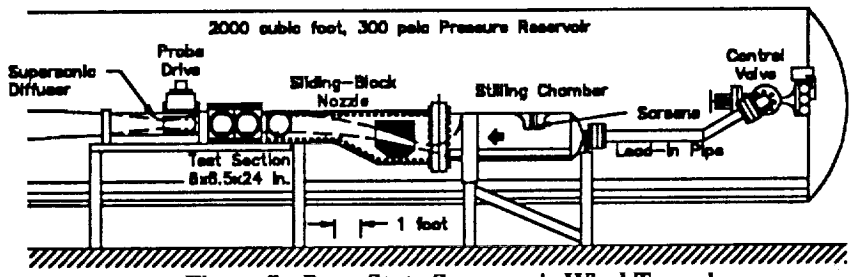

Figure 7 - Penn State Supersonic Wind Tunnel.

Calibrations of the flowfield have shown excellent flow quality. The maximum deviation in Mach number across the test section has been shown to be 2%. The Reynolds number of the facility ranges from a low of 6.5×10^7 at Mach 4.0 to a high of 1.0×10^8 at Mach 1.5.

A separate high pressure air line was constructed for this study. A schematic of the system is shown in Figure 8. This system uses as its supply either the wind tunnel pressure reservoir, an auxiliary tank, or high pressure gas cylinders. A 4 kW in-line immersion heater, upgradable to 18kW, is used to control the total temperature of the injected stream.

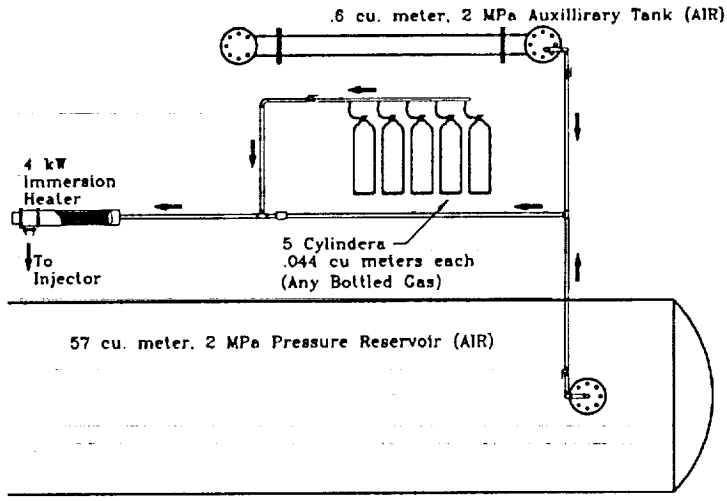

Figure 8 - High pressure gas injection system

3.1.2 Penn State Gas Dynamics Lab - Optics Lab

The Optics Lab houses equipment used for optical diagnostics. It also contains a research area where new techniques may be proven before being attempted in the wind tunnel environment. In addition, a portion of the lab contains the free-jet test stand used for calibrations and testing. This free jet uses the same high pressure air supply as the supersonic wind tunnel.

3.1.3 Vortex Injector

A vortex injector was designed and built specifically for this research. A picture of the finished injector is shown in Figure 9 and a drawing of the injector installed in the tunnel is displayed in Figure 10. The coordinate system used in this study is shown in Figure 11. The injector consists of an 1.78 cm (0.70 in.) ogive-cylinder forebody mounted on an 8% thick bi-convex airfoil. High pressure air is supplied to the forebody though the hollow strut. The incoming air is conditioned by means of a tube-bundle flow straightener. If desired, the flow may have swirl added to it by means of 4 interchangeable sets of swirl vanes. These computer-designed swirl vanes are pictured in Figure 12. The vanes, which are designed to produce a potential vortex (rv_θ = constant) away from the viscous core, yield flow angles of 15, 30, 45 or 60 degrees at the hub exit. Four interchangeable nozzles, pictured in Figure 13, are threaded to attach to the forebody. The nozzles are method-of-characteristics designs for Mach 2.6, 3.1, 3.6 and 4.0 air flow (gamma = 1.4) with no boundary layer correction. The contours of the nozzles also yield good flow quality for other gases. The plenum of the injector is instrumented to measure pressure and temperature. The boundary layer on the outside of the injector has been measured to be .35 cm (.14 in.) thick while the boundary layer on the inside of the nozzles is of negligible thickness. A spark-schlieren photograph of the boundary layer is shown in Figure 14.

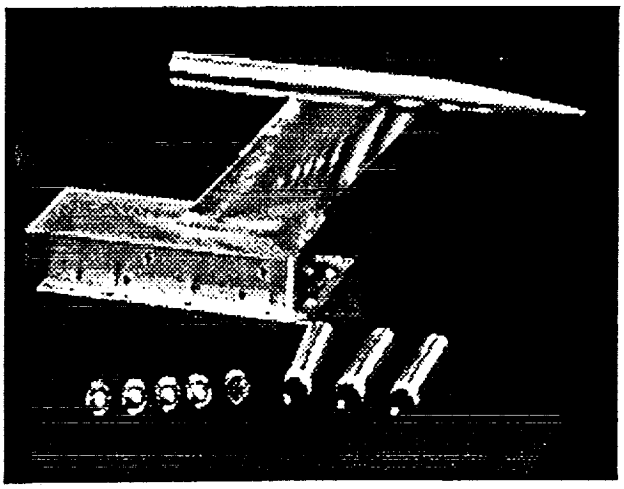

Figure 9 - Vortex injector, swirl vanes and nozzles.

Figure 10 - Drawing of injector installed in the wind tunnel. Design features are highlighted.

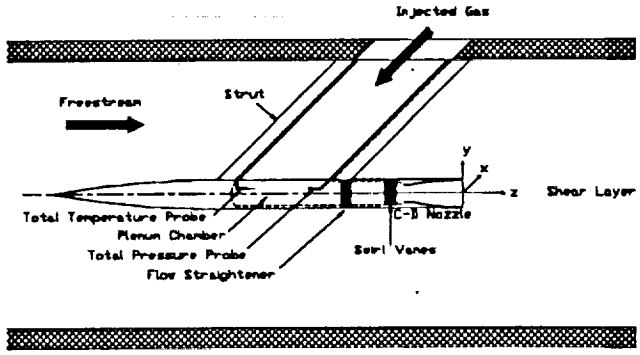

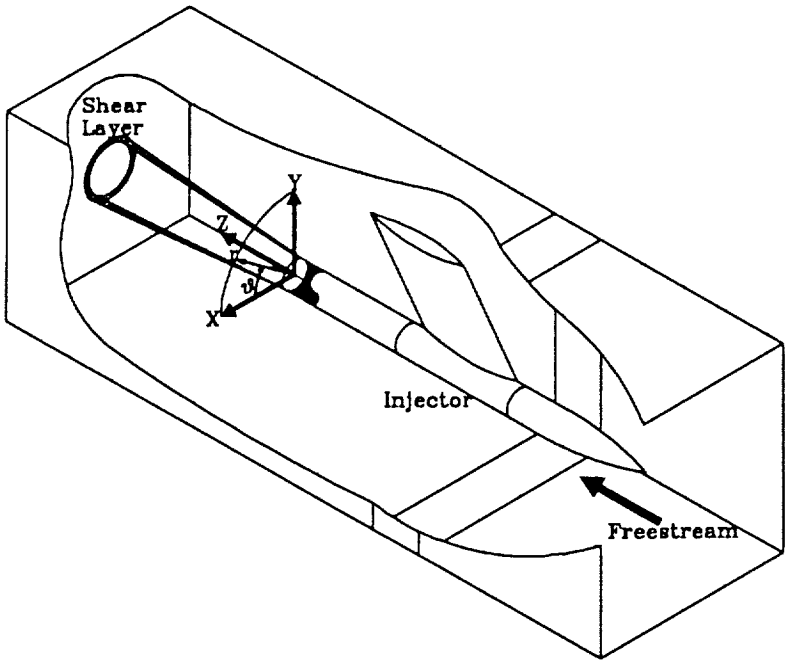

Figure 11 - Injector installed in tunnel showing coordinate system used.

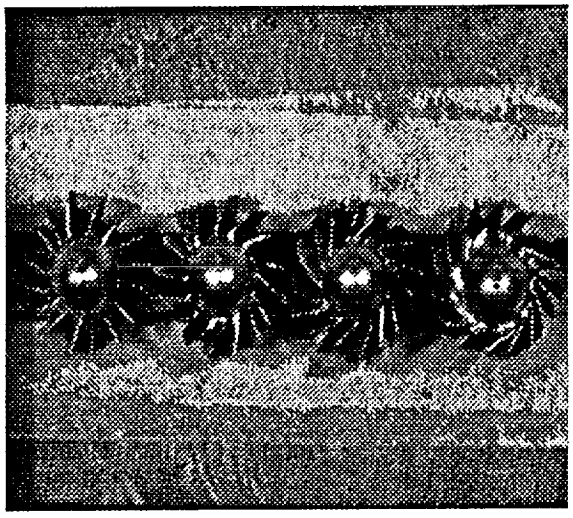

Figure 12 - Navier-Stokes-designed swirl vanes. From left to right are the 15, 30, 45, and 60 degree vanes.

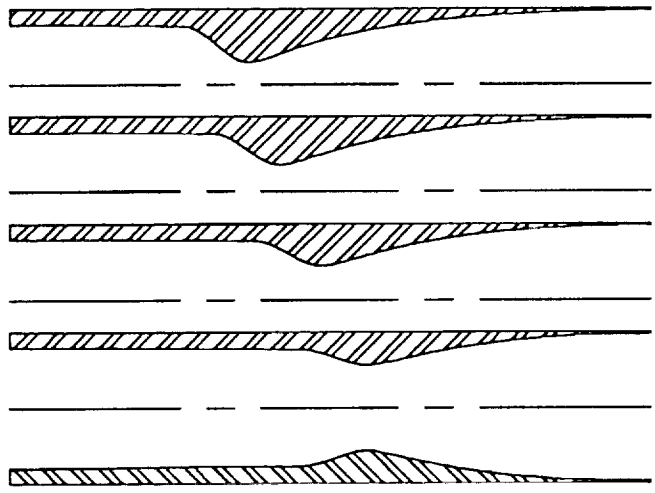

Figure 13 - Method-of-characteristics designed nozzles. From top to bottom are Mach 4.0, 3.6, 3.1 and 2.5 designs for air.

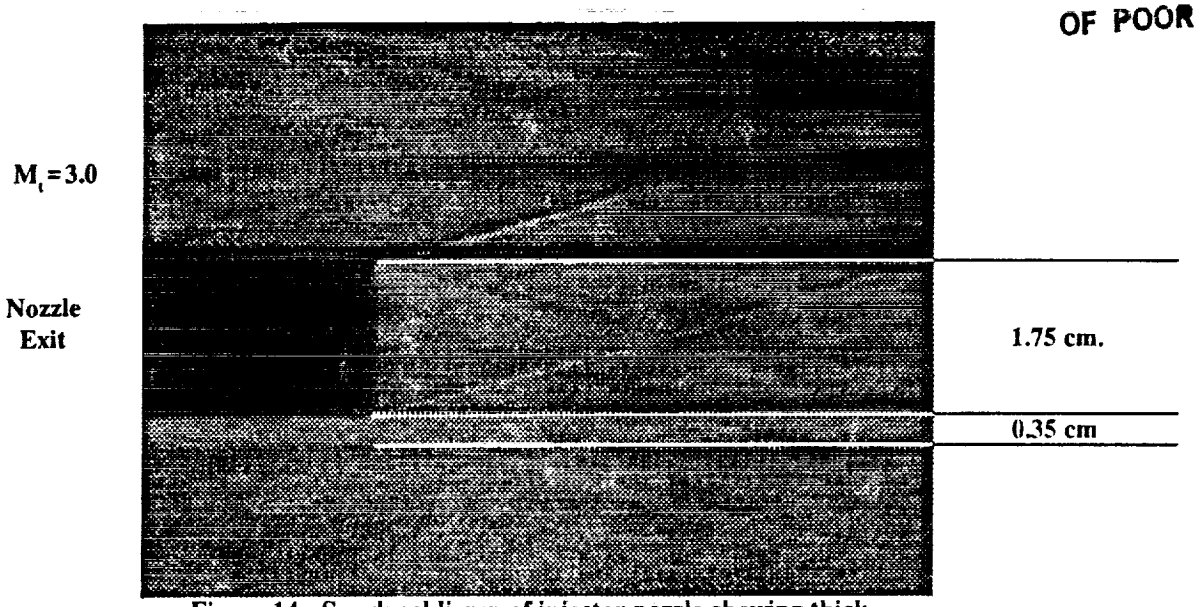

Figure 14 - Spark-schlieren of injector nozzle showing thick boundary layer on the trailing edge. Flow is from left to right in the picture.

3.2 EXPERIMENTAL METHODS

Both intrusive probe surveys and non-intrusive optical investigations of the flowfield were made. Below, each of the techniques used is briefly discussed.

3.2.1 PROBES

3.2.1.1 Five-Hole Probe

A five-hole probe was used to measure total pressure, Mach number, and flow angularity in several flowfields. The probe used was a miniature, fast-response probe shown in Figure 15. The design and calibration of this probe is explained in detail by Naughton *et al*[55](1991); pertinent characteristics are listed in Table 1. The advantages of such a probe are that it measures total pressure, Mach number and flow angularity at each point where data is taken. In addition, the small tip diameter allows for excellent spatial resolution. The disadvantage of probe surveys is that a complete flowfield survey requires multiple runs. Also, the probe has a limited range of Mach number and flow angularity for which the calibration is valid, and it is only valid for air. It also cannot probe flows, such as vortex breakdown, where its intrusive nature could affect the flowfield.

3.2.1.2 Total Temperature Probe

Figure 16 shows the design of the total temperature probe used, a Beckman Series 300 miniature thermocouple specially modified for supersonic flow. The junction is a micro-disc with

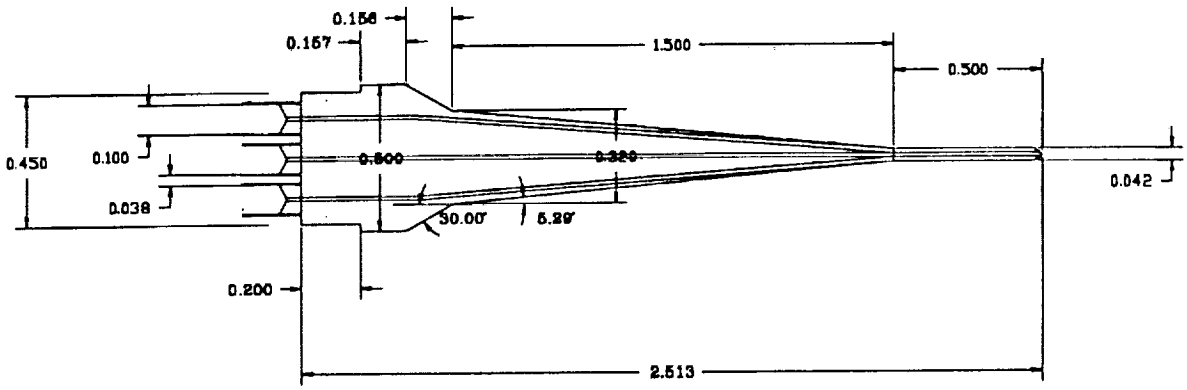

Dimensions in inches

Figure 15 - Five-hole probe drawing.

Five Hole Probe Characteristics	
Probe Tip Diameter	1 mm (0.042 in.)
Tip to Transducer Distance	64 mm (2.513 in.)
Pressure Transducer Frequency Response (uninstalled)	~270 kHz
5-Hole Probe Frequency Response (transducers installed)	~50 Hz
Pressure Transducer Temperature Compenstion Range	-54 to 121 C
Pressure Transducer Range	0-350 kPa (0-50 psia)
Pressure Transducer Full Scale Output	300 mV
Mach Number Calibration Range	2.0 - 4.0
Flow Angularity Range (degrees)	Pitch 0 - 25 Roll 0 - 360

Table 1 - Pertinent 5-hole probe characteristics

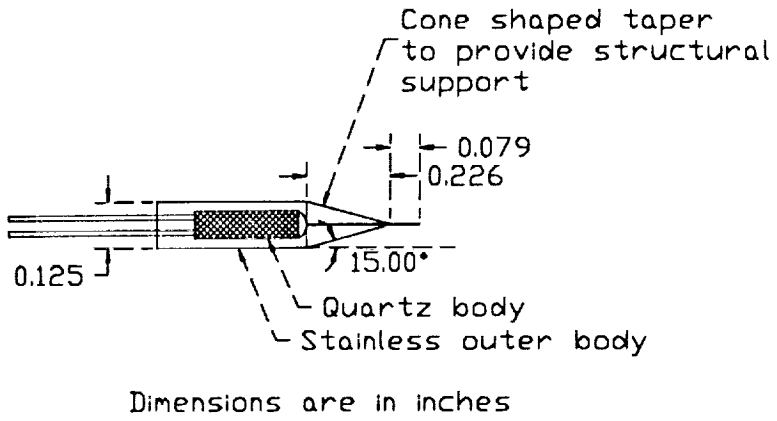

Figure 16 - Modified Beckman series 300 total temperature probe.

nominal dimensions of 75-100 microns (.003-.004 in) in diameter and 2.5-7.5 microns (.0001-.0003 in.) thick. The frequency response of this probe is sufficient to take data continuously while the probe is moving (at approximately 1 cm/sec) through the flowfield; thus, surveys can be completed quickly. However, this remains a time-intensive process and cannot be used where the intrusive nature of the probe could affect the flowfield.

3.2.1.3 Probe Drive

Both the probes are positioned in the flowfield by a stepper-motor-driven probe drive. The probes are mounted to a sting which attaches to a strut that may moved. The stepper motors allow for movement in increments as small as 6.5 microns (1/4000 in.). The stepper motors control positioning along two orthogonal axis in the crosstream plane of the wind tunnel. The streamwise position is determined by adjusting the sting position in the strut.

3.2.2 OPTICAL DIAGNOSTICS

3.2.2.1 Schlieren

The schlieren system used was a conventional Z-type schlieren with two extra folding mirrors added for space limitation reasons. This type of visualization was used primarily to insure flow quality and to estimate the boundary layer thickness on the vortex injector. Since the schlieren method spatially integrates over the test section, it was not used to measure mixing rates due to the 3-D nature of this flow.

3.2.2.2 Planar Laser Scattering Imaging

Planar Laser Scattering (PLS) flow visualization has been used successfully in both low-speed (Kegelman[56](1986)) and high-speed flows (Clemens and Mungal[57](1991)). The setup is shown in Figure 17. The beam from a 10 Watt pulsed Cu-vapor laser is directed to an optical beam mounted on a traversing system. In this way the sheet of laser light created by the optics, shown in detail in Figure 18, may be positioned anywhere in the test section and may be scanned along the length of the test section during a run by stepper motors. To record the PLS image, a camera is mounted on a separate traversing system. When the sheet of laser light moves, the camera moves parallel to it in order to keep the image in focus at all times.

The light-sheet optics consist of two spherical and two cylindrical lenses as shown in Figure 19. The spherical lenses are used to control the location of minimum sheet thickness, while the cylindrical lenses control the extent of the sheet. Depending on the camera used, either multiple pulses or a single pulse of the laser could be captured on each frame.

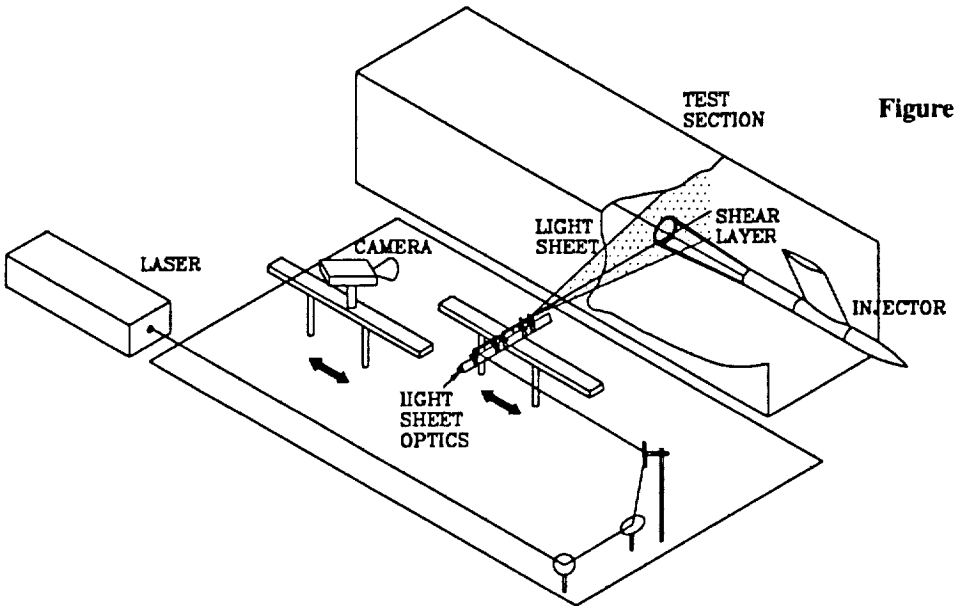

Figure 17 - Planar Laser Scattering (PLS) setup.

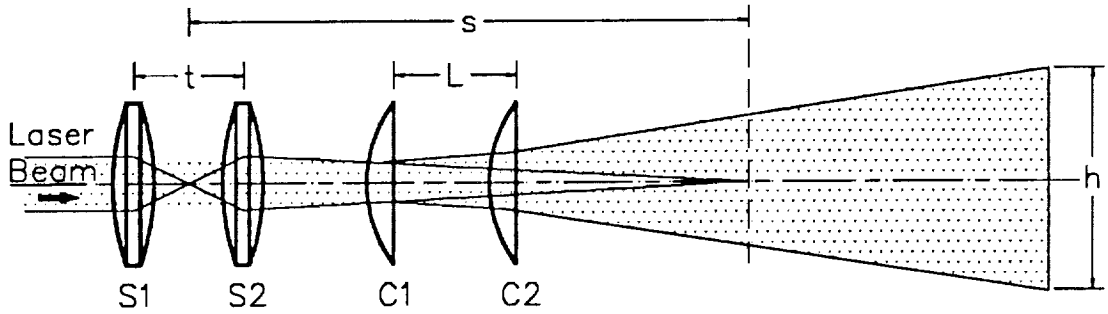

Figure 18 - Detail of PLS optical setup.

This technique has the advantage of surveying the entire flowfield in 1 run. For the camera magnification used, each pixel of the image represented $1x10^{-4}$ sq. cm. (1.5×10^{-5} sq. in.), yielding excellent spatial resolution for this flow. However, processing these images for quantitative information is a new area and proved to be a formidable task.

The particles utilized for scattering the laser light are created by allowing a trace amount of water vapor to exist in the high pressure tank. Upon expanding through the nozzle the temperature drops a sufficient amount for the water vapor to crystallize. It is these ice particles that are the scattering centers for the laser light. Alvi and Settles[58](1991) present a detailed discussion on measurement techniques used to determine particle size in this facility. They determined a value of 0.4 microns as the upper limit on the particle diameter. However, these results are only approximate upper limits, and other researchers have suggested that these particles may be much smaller than the maximum sizes measured.

The size of the scattering particles is important for two reasons. First of all, the particle Reynolds number, $Re_p = (|u_p - u_f| * D_p)/\nu$, must be sufficiently small in order for the particles to faithfully follow the flow. This requires small-diameter particles. However, the particle diameter must be large enough to scatter the incident laser light, so the particles must not be too small. Several methods of addressing this issue have been used in the past by different researchers. Goebel and Dutton[14](1990) varied the particle size between 0.3 micron titanium oxide and 0.5 micron polystyrene-latex (PSL). Since they found little difference in their measurements, they concluded that their particles were tracking the flow. Samimy and Lele[59](1990) tracked particles in a computationally-determined shear layer. They found that the important parameter was the Stokes Number, $St = \tau_p/\tau_f$. They determined that only the smallest particles followed the flowfield. They suggested that, since velocity-bias error effect on the particle location is cumulative, the requirements on particle size for planar light scattering were much more restrictive for PLS than for LDV. Maurice[60](1991) analyzed particles in a vortex flow. He modeled the flow with an inviscid, potential vortex, and with the results of a Navier-Stokes computer solution. He found that only silicon oil particles of 0.1-0.2 microns tracked the flow for both models.

3.3 DATA ACQUISITION SYSTEM

3.3.1 Configuration

The setup for the data acquisition system is shown in Figure 19. The signal conditioned output of transducers is input to a filtering system. The filters used are 6-pole, 6-zero elliptic low pass filters with 80 dB per octave pass-band attenuation. The filtered output is then routed to the

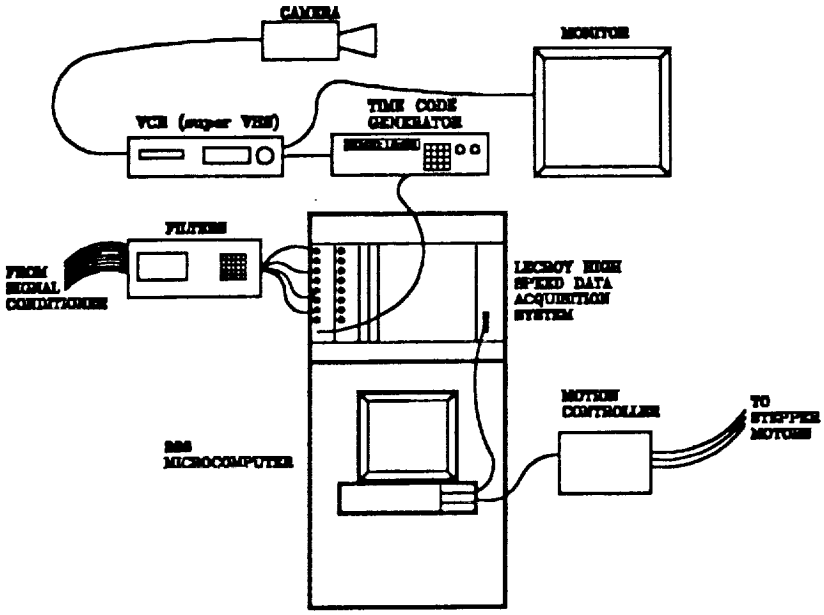

Figure 19 - Data acquisition configuration

LeCroy high speed data acquisition system. This system consists of 3 waveform recorders with 4 channels each. The data may be sampled at discrete frequencies between 20 Hz and 5 MHz and is stored in a 512 K circular buffer. This entire system is controlled by a 386 microcomputer.

The video system uses either a super-VHS video camera or a Xybion low-light-level camera. The Xybion camera contains a micro-channel plate intensifier that can detect light intensities as low as 1 millionth of a footcandle. Each frame may be gated through the intensifier at 20 msec to 25 nanoseconds. With the appropriate gating, a single pulse from the Cu-Vapor Laser is captured on each frame. The output from either camera is routed to a super-VHS video cassette recorder. In order to coordinate video data with the digitized transducer data, a time code generator records the run time on the tape. The time signal may be recorded directly on the screen for composite signals or on the sound track of the tape for super-VHS recordings. The sound track signal may be read during playback and appears on the time code generator display. This allows for a coordinated time base between video images and transducer records.

During any given run, the PLS optics may remain at a fixed position or may be traversed axially along the test section. The PLS optics positioning and traversing is regulated by a motion controller.

3.3.2 Probe Survey Acquisition Process

For a typical run, the wind tunnel is brought to steady-state conditions before the data acquisition is triggered. Upon triggering, the data acquisition begins sampling and the motion

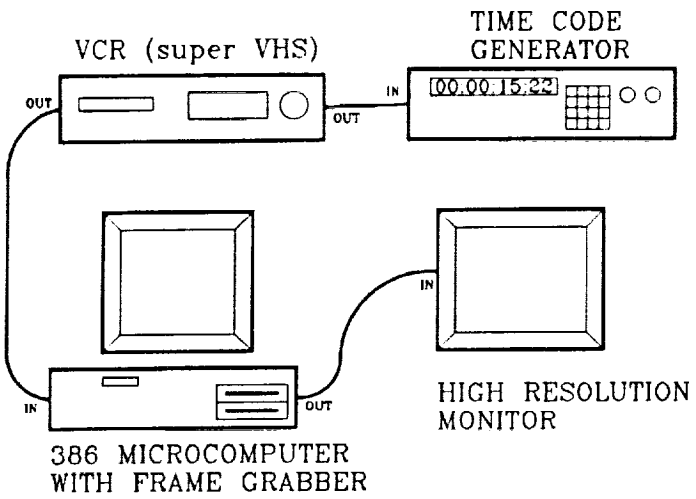

Figure 20 - Image acquisition hardware.

controller moves the probe through the tunnel in a predetermined manner. At the completion of a run, data is downloaded from the digitizer buffer to the host computer.

3.3.3 Laser Light Sheet Data Acquisition Process

For runs where video images of the light sheet are taken, the process is slightly different. The VCR begins to record and the wind tunnel is brought to steady-state conditions. The host computer then triggers the LeCroy data acquisition system and simultaneously the motors begin to traverse the light sheet. When the LeCroy is triggered, it sends a trigger to the time code generator to begin incrementing. In this way, the data taken by the LeCroy may be synchronized with the images recorded on the VCR.

3.4 IMAGE DIGITIZATION

3.4.1 Hardware

The configuration of video hardware used to grab images from video tape is shown in Figure 20. Much of the hardware is the same as that used in image acquisition with the addition of the frame grabber. The frame grabber is a plug-in board to the microcomputer with 1 megabyte of memory. This allows for the storage of up to four 512 x 512 images. The board may be accessed via menu-driven software or FORTRAN subroutines.

3.4.2 Image Grabbing Process

Images are digitized in the following manner. The VCR is advanced to the desired location and is paused. At this point, the time code generator displays a time corresponding to the displayed image. The exact position on the tape may be changed by frame advancing. When the proper image is located, an image is grabbed and stored to disk for future processing.

4. DATA ANALYSIS

4.1 Probe Data Reduction

4.1.1 Total Temperature Data Analysis

The signal measured during a total temperature survey is actually the recovery temperature of the probe tip. The total temperature is greater than the measured temperature by some factor determined by Mach number; however, this factor does not vary a great deal. Determination of this factor versus Mach number is performed by measuring a known total temperature, say in the wind tunnel freestream; the ratio of the known temperature to the measured temperature is the correction factor. Repeating this over a wide range of Mach numbers yields a curve of recovery factor versus Mach number. If Mach number is known from five-hole probe results in the region in which temperature measurement occurred, then this correction may be applied at each point measured.

In order to compensate for the variation with respect to time in stagnation temperature of both the wind tunnel and the injected flow during a given run, a non-dimensional temperature, theta, is used. This non-dimensional temperature, θ, is given by:

$$\theta = \frac{(T_{o,p} - T_{o,t})}{(T_{o,i} - T_{o,t})} \qquad (1)$$

For the total temperature runs, the injected flow was heated to a total temperature above that of the wind tunnel. Thus, if the probe total temperature, $T_{o,p}$, is that of the injected stream, $T_{o,i}$, then θ will be unity. On the other hand, if the probe total temperature corresponds to the tunnel stagnation temperature, $T_{o,t}$, then θ will be zero. Thus theta is a measure of the relative temperature of a given point in the flow with respect to the freestream and injected flow temperatures.

4.1.2 Five-Hole Probe Data Reduction

The data reduction process is discussed in detail by Naughton *et al*[55](1991). The data reduction process follows the method of Centolazi[61](1957). This entire scheme has been programmed in FORTRAN for immediate reduction after testing. The results of this data-reduction process are the total pressure, Mach number and flow direction at measured points in the flowfield. The errors associated with each of these quantities are listed in Table 2.

4.1.3 Combined Probe Results

The combination of the five-hole and temperature probes results allows the calculation of any mean flowfield variable. Successful use of these quantities to calculate mass flow and energy flow per unit area was made by Naughton *et al*[44](1989). Integrated across the jet, these quantities yield mass and energy entrainment.

Error		Mach Number	Total Pressure (%)	Static Pressure (%)	Roll (deg)	Pitch (deg)	Mx	My	Mz
M=2	Mean	0.07	6	5	4.3	0.5	0.02	0.02	0.06
	RMS	0.07	6	5	5.9	0.7	0.02	0.02	0.07
	Max	0.09	7	8	19.4	1.8	0.04	0.04	0.09
M=3	Mean	0.05	4	6	0.6	0.4	0.02	0.02	0.04
	RMS	0.07	4	6	1.2	0.5	0.03	0.03	0.06
	Max	0.18	14	12	11.1	1.5	0.10	0.10	0.17
M=4	Mean	0.08	6	6	1.9	0.4	0.03	0.03	0.07
	RMS	0.11	8	7	3.6	0.5	0.04	0.04	0.10
	Max	0.26	23	13	14.7	1.5	0.12	0.12	0.24

Table 2 - 5 hole probe errors

4.2 Laser Light Sheet Image Analysis

4.2.1 Background

The use of light scattering techniques to evaluate concentration levels is not a new technique. Rosensweig *et al*[62] explored this technique as early as 1960. They focused a light beam in a low-speed jet and measured the intensity of scattered light from smoke particles seeding the flow. From these intensities, they calculated mean density profiles, concentration fluctuations, spectral densities and two-point correlations. Schneiderman and Sutton[63](1969) imaged the wake behind a cone in supersonic flow. By seeding the wake with smoke particles, enough light was scattered so that with an image intensifier they were able record the image on high speed film. From the resultant images, they calculated mean concentration profiles, spectral densities, and two-point correlations. The results from these calculations agreed well with other measurement results, such as those from hot wire anemometry. Chao *et al*[64](1990) scanned a laser beam across a low-speed jet seeded with smoke particles. They recorded the images on a CCD camera and were able to

calculate the width, convective velocity, and instantaneous concentration maps of the jet. Thus, it seems well established that light scattering from particles can yield sufficient information to calculate mixing areas from laser sheet images.

4.2.2 Data Reduction Process

A computer program was written to analyze the digitized images of the scattered laser light. Details of the program are given below. An overview of image processing techniques, such as those used in the data reduction program, may be found in texts on the subject such as those of Gonzalez and Wintz[63](1987) and Schackoff[64](1989). The final program is the result of trial and error process since several schemes used to extract mixing information from the images were either entirely unsuccessful or had variations in results from image to image that were unacceptable. The final scheme requires approximately 4 minutes of computation time per image on a 386 microcomputer. A roadmap of the image analysis program is shown in figure 21. Each step is discussed briefly below.

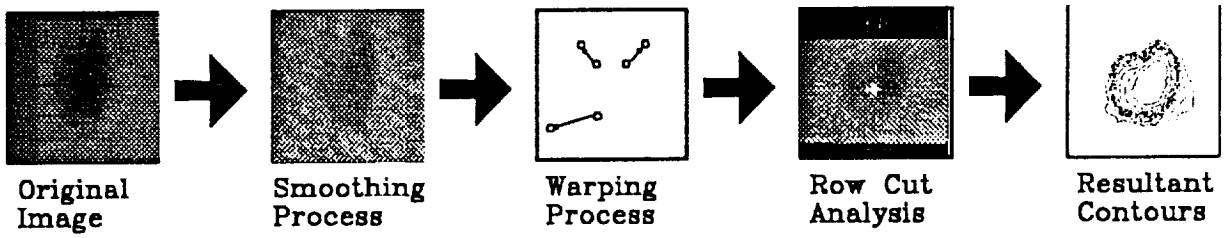

Figure 21 - Roadmap of image analysis process.

4.2.2.1 Smoothing

The first image manipulation is a smoothing process to eliminate noise in the images. Such noise can arise from several sources: seeding density fluctuation, variation in laser power, camera induced noise, VCR recording noise, and VCR to frame grabber noise. Repeated smoothing is made in order to obtain a reasonable image. The reduction in noise for a given row in an image due to this process is illustrated in Figure 22. Although the high frequency noise is eliminated, the large gradients of interest are unchanged.

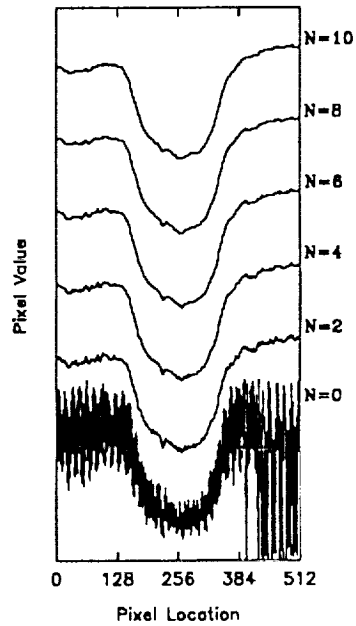

Figure 22 - Effect of repeated smoothing on noise in image

4.2.2.2 Spatial Warping

Figure 18 shows that the camera view is not normal to the laser sheet. In order to calculate a directionally-unbiased result, this viewing direction must be accounted for. This is accomplished by means of a spatial warping or mapping using an image of a grid taken from the same angle as a reference. Three points are selected from the imaged grid and mapped into three new locations such that the resultant image will contain squares with an equal number of pixels on all sides. With three initial points, (x_1,y_1), (x_2,y_2), (x_3,y_3), and three destination points, (x_1',y_1'), (x_2',y_2'), (x_3',y_3'), selected, equations for the mapping may be written:

$$x_1' = a_1 + a_2 x_1 + a_3 y_1 \qquad 2(a)$$

$$x_2' = a_1 + a_2 x_2 + a_3 y_2 \qquad 2(b)$$

$$x_3' = a_1 + a_2 x_3 + a_3 y_3 \qquad 2(c)$$

By simultaneously solving equations 2(a), 2(b) and 2(c), the unknown coefficients, a_1, a_2 and a_3 are determined. In a similar manner, the coefficients for y' are determined. Knowledge of these constants allows all points in the original image to be mapped to their new location.

4.2.2.3 Radial Cut Analysis

The final step in the processing is the radial cut analysis. The images are first cut radially in 60 separate rays (Figure 23a), and the pixel values along these rays are stored in vectors (Figure 23b). The pixel values in this vector range from a minimum in the unseeded center of the jet, to a maximum in the seeded exterior flow. Each one of these vectors is normalized between zero, the pixel value at the center point, and unity, the maximum pixel value found in the freestream. Then the location of a given intensity level is located and its spatial position determined (Figure 23c). By connecting all the spatial locations of a given intensity level from each of the 60 rays, a contour of that intensity value is determined. The area within this contour is then determined simply by counting the pixels within it.

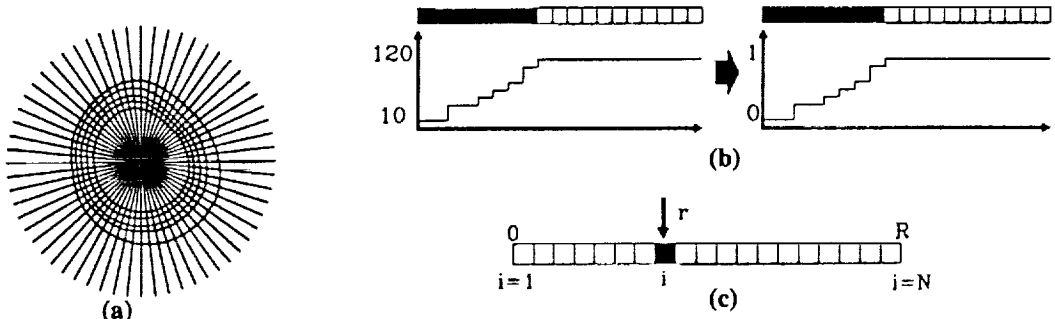

Figure 23 - Radial cut process. (a) radial cuts (b) example vector being normalized (c) locating given intensity level.

The results of each step of the image analysis process are shown in Figure 25. The contours shown in Figure 25(d) are from 0.10 to 0.90 in 0.10 increments.

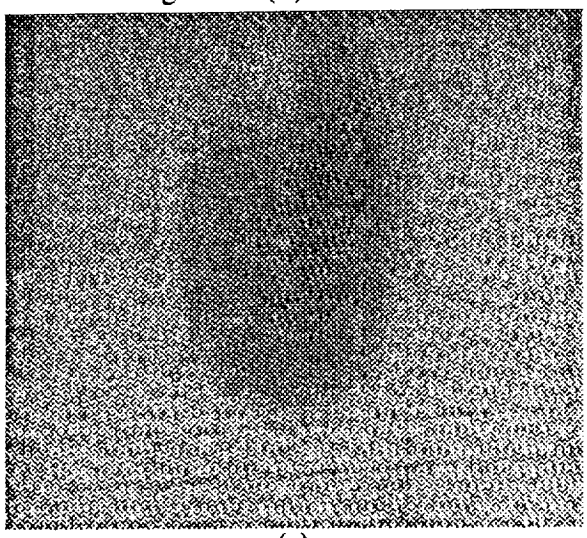

(a)

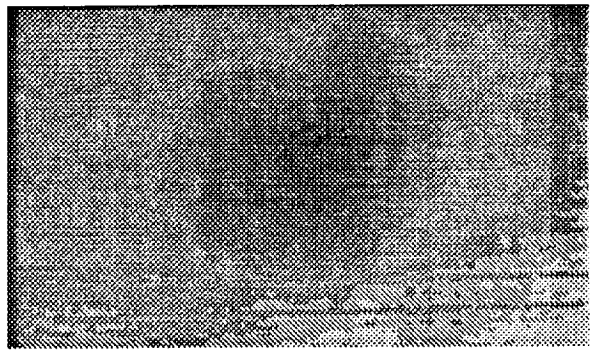

(b)

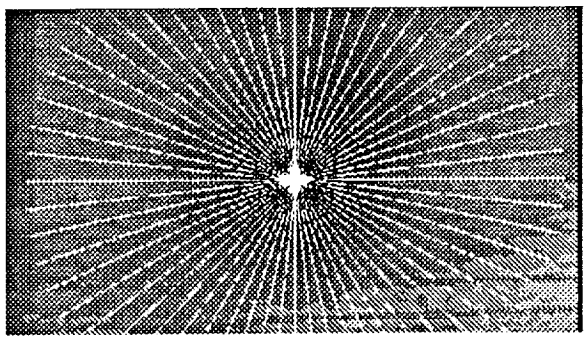

(c)

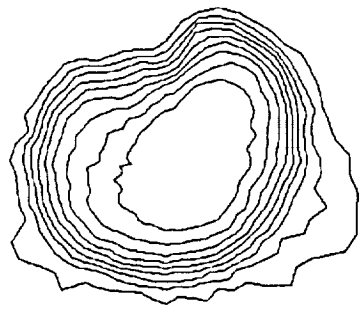

(d)

Figure25 - Results of radial cut analysis.
(a) original image (b) smoothed, warped image (c) radial cuts (d) intensity level contours.

4.2.3 Jet Terminology

Before discussing the results of this image analysis, a clarification of terms is necessary. Figure 26 shows a cross-section typical of the injected flows in this study. A_i represents the area within a given intensity contour and r_i is the radius of a circle with the same area. A_{mix} represents the difference of the are of two intensity contours, A_o, the area within the outer contour, and A_i, the area within the inner contour ($A_{mix} = A_o - A_i$). The equivalent shear layer thickness for the 3-D flow, delta, is calculated by determining the radii, r_o and r_i of two areas, A_o, and A_i, and calculating the difference. Finally, when the term "jet" is used in discussing the data, it represents a case without swirl. When the term vortex is used, it refers to a swirling case (i.e. a set of vanes is used).

4.2.4 Image Reduction Error Analysis

In order to determine the accuracy of the results of the image analysis, an in-depth error analysis was performed. This analysis was statistical in nature and accounted for all errors and variability during a given run; however, this analysis did not account for bias errors. The results of the image analysis for fifty different images at the same test conditions were averaged for a jet case at L/D = 3 and 9. In addition fifty images were also reduced and for the vortex case at L/D = 9. This allowed for evaluation of statistical errors for the following quantities: A_i, A_{mix}, $A_{mix,vortex}/A_{mix,jet}$, and $\delta_{vortex}/\delta_{jet}$. The relative errors calculated for these quantities are summarized in Table 3. These errors represent the standard deviation of the given quantity over the fifty images. Notice that errors associated with the 0.9 contours are large; this is due to the fact that the slope of the intensity curve is flattening as it approaches 1.0 and thus the 0.9 boundary is very sensitive to any variations in freestream intensity.

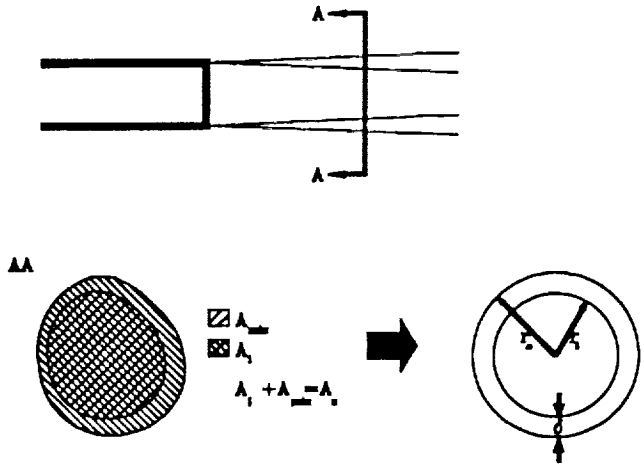

Figure 26 - Jet Terminology

Contour Level	0.1	0.2	0.3	0.4	0.5	0.6	0.7	0.8	0.9
Error	0.068	0.033	0.017	0.010	0.009	0.008	0.008	0.012	0.024

Table 3 - Image analysis error summary . (a) gives errors associated with the area of a discrete contour levels.

Contour Pairs	.1 - .9	.2 - .8	.3 - .7	.4 - .6
A_{mix} Error	.037	.026	.025	.023
$A_{mix,vortex}$ /$A_{mix,jet}$ Error	.043	.038	.048	.053
δ_v/δ_j Error	.063	.052	.057	.060
$d(\delta_v/\delta_j)/d(L/D)$ Error (absolute)	.0096	.0080	.0087	.0090

Table 3b - Image analysis error summary. summarizes errors associated with quantities involvin two contour levels. All errors are relative unless noted.

5. RESULTS

5.1 Test Matrix

Table 4 lists the different cases that were run. In all, 11 vortex and 7 jet cases were run covering a convective Mach number range from 0 to almost 2. This large range of convective Mach number is made possible by using different injection gases. The results represent over 500 individually-reduced images. It is important to note that the convective Mach number listed in the table is for the no-swirl case. The actual swirl imparted to the flow is a function of both the swirl vanes and nozzle used since the swirl vanes impart the tangential velocity upstream of the C-D nozzle. If the tangential momentum is fixed, then the ratio of tangential momentum to axial momentum (one definition of swirl) depends upon the axial momentum produced by the nozzle.

Tunnel Mach Number	Injector Mach Number	Gas	Vane Angle			Convective Mach Number	Comments
			30	45	60		
3.5	2.60	AIR	x	x	x	0.15	
3.5	3.60	AIR		x		~0	Vortex Breakdown
3.0	3.10	AIR		x		~0	
4.0	2.84	He-N2		x		0.7	
4.0	2.95	He	x	x	x	1.3	
4.0	3.68	He		x		1.6	
4.0	4.49	He		x		1.9	

Table 4 - Test Matrix

5.2 Five-Hole Probe Survey Results

A representative result from the five-hole probe is shown in Figure 26. These results are for $M_t = 3.0$ and $M_i = 3.1$ with the 30 degree swirl vanes. This survey was taken at $L/D = 5.35$. Since this cut is through the center of the vortex, the cartesian components of the Mach number, M_x and M_y, are the same as M_r and M_θ. The curve fit of the tangential Mach number (the solid line in Figure 26) is an Oseen vortex form:

$$M_\theta = (k/r) * (1 - e^{\frac{-r^2}{r_a^2}}) \qquad (3)$$

The curve fit is only fitted for half the vortex since axisymmetry is assumed. The curve fit fails at the outer edge of the vortex due to the effect of the shear layer.

Results for the test matrix of Table 4 are not yet presented due to several problems. First, the swirl cases in which air was the injectant gas proved to be extremely strong vortices. The gradients were so steep in the core of the vortex, that no reasonable results were attainable. Secondly, the helium vortex could not be measured because the 5-hole probe is only calibrated for air. This leaves unfinished the quantification of swirl, a critical part of this study. This item is addressed in the conclusions.

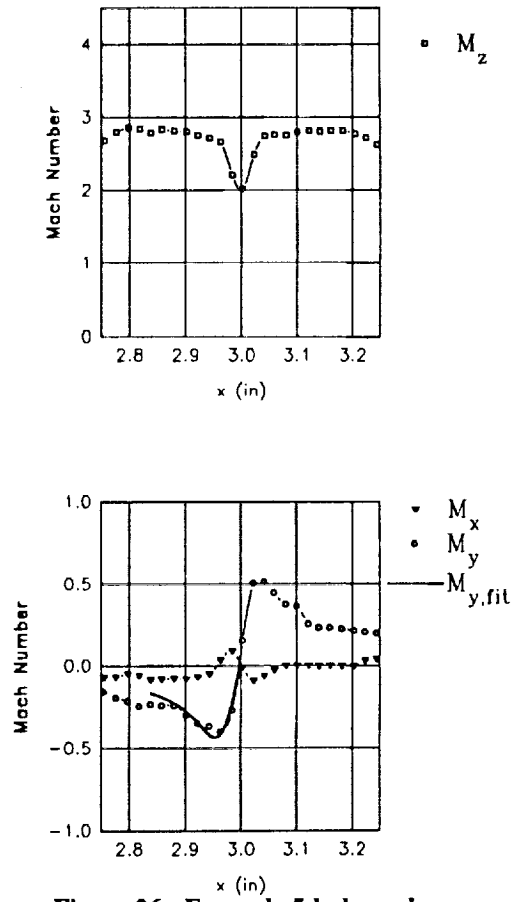

Figure 26 - Example 5-hole probe results.

5.3 Total Temperature Survey Results

The survey results for a jet case with air, M_t=3.5, M_i=2.6, L/D=9.0, are shown in the contour plot of theta in Figure 27(a). Figure 27(b) is for the same conditions except that 45 degree swirl vanes were installed. The total temperature of the probe, $T_{o,p}$ used in the calculation of theta was determined from the measured recovery temperature on the probe tip, $T_{r,p}$. This recovery temperature was multiplied by a constant, $T_o/T_{r,p}$, calculated in the Mach 3.5 freestream. This approach is used since the Mach number at all points in the flow is not known.

The jet results yield the typical "top hat" profile, indicative of a heated injected stream. However, vortex contours of theta are significantly different. The total temperature in the "wings" of the vortex are higher than would be expected, and the total temperature in the core drops dramatically. This phenomenon of total temperature separation was first discovered in a Ranque-Hilsch vortex tube. Deissler and Perlmutter[67](1960) attribute this "energy separation" to shear work performed by the vortex core on the outer region of the vortex.

5.4 Image Analysis Results

5.4.1 Contour Areas

The areas contained within given contour levels, non-dimensionalized by the nozzle exit area, are shown in Figure 28(a) for the jet and Figure 28(b) for the vortex. The conditions for this case were M_t=4.0, M_i=2.84, 80% Helium 20% Nitrogen injection, which yields a convective Mach

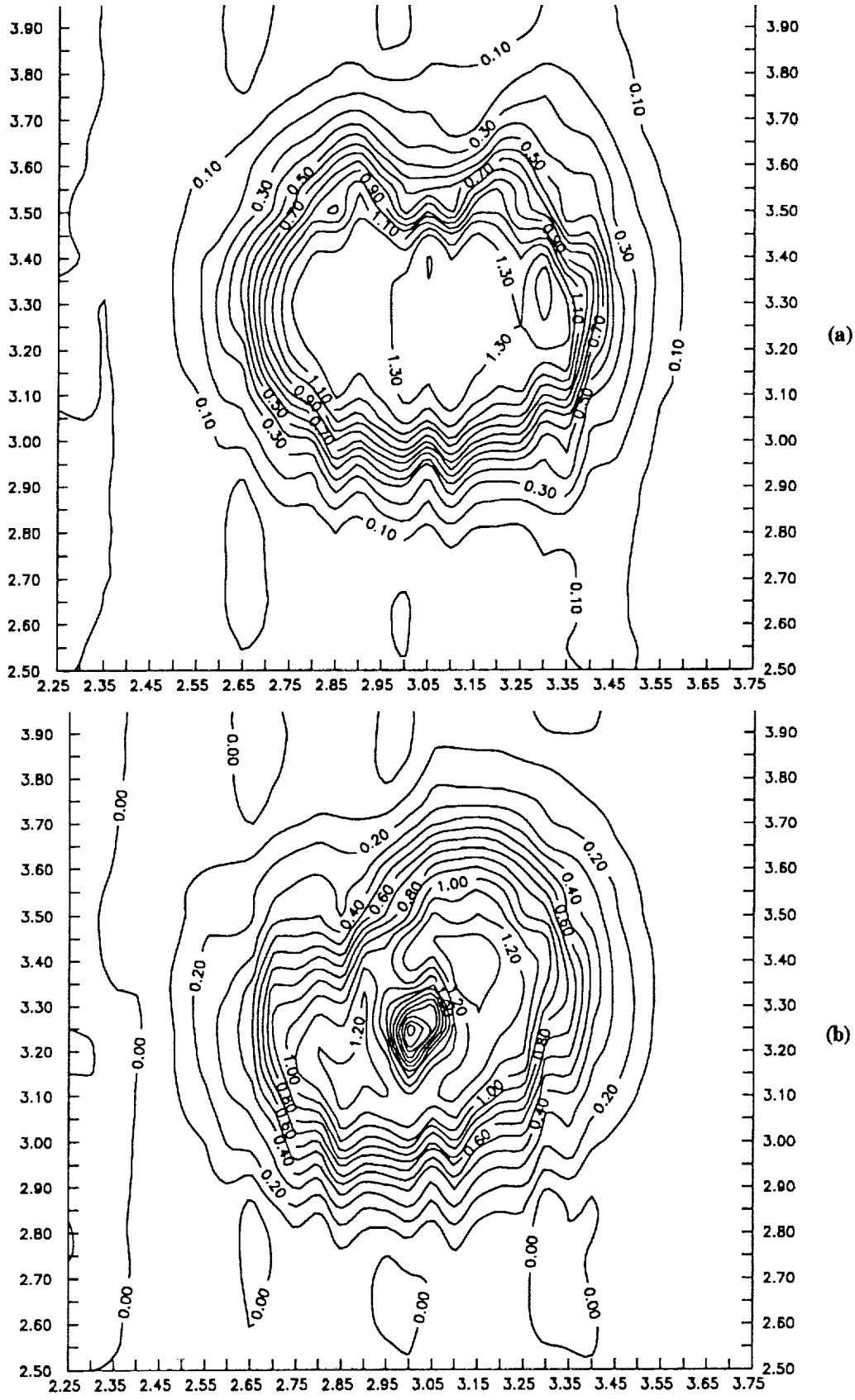

Figure 27 - Contours of theta. (a) Jet case $M_{j=2.6}$
(b) Vortex Case $M_{j=2.6}$, $\theta = 45°$

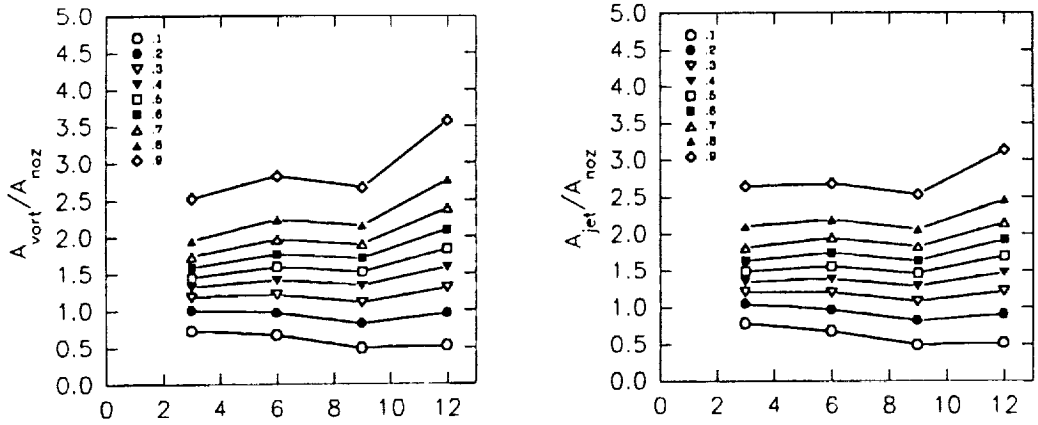

Figure 27 - Areas within a given intensity contour as a function of distance downstream (a) vortex, (b) jet.

number of 0.7. For the vortex case 45° vanes were inserted. It is reasonable to expect non-dimensionalized areas contained within all contours should extrapolate to 1.0 at L/D = 0 since the shear layer should be infinitely thin at the nozzle exit. In this limit, all the intensity contours should stack up, appearing as a circle with a radius equal to that of the nozzle exit. (In this case all the contours would contain an area equal to that of the nozzle exit area.) In the Figure, we see the innermost contour extrapolating to about 1.0 at L/D = 0, but the outermost contour is approaching about 2.0. One explanation for this observation is that a near-field effect is causing the 0.9 contour to grow large by L/D = 3; however, the inner boundary does not show a similar near-field-growth effect. A more plausible explanation is that the shear layer has an initial intensity distribution at the nozzle exit. This intensity distribution, it is proposed, is due to the thick boundary layer that develops on the ogive-cylinder body. The approximate size of the boundary layer is seen in Figure 14, a spark schlieren of the nozzle. The lack of an initial intensity distribution inside the nozzle exit radius is due to the fact that there is no seeding in the injector flow. The outer perimeter of the boundary layer encompasses an area of approximately 2.0 nozzle exit areas. This agrees very well with the calculated results.

The evolution of the different A_i's with distance downstream appears qualitatively correct. The inner contours appear to be moving inward with distance downstream and the outer contours

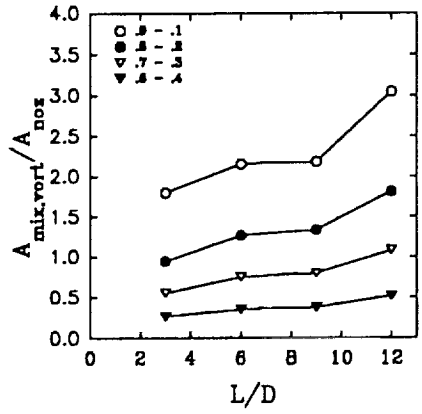

Figure 29 - Mixing area between two intensity level contours.

are growing outward. However, the rate at which the jet contours are diverging is smaller than that of the vortex.

5.4.2 Mixing Areas

The goal of this study is to evaluate the mixing of a given vortical flow and compare it to a jet flow. Thus, it is imperative that the measure of mixing is consistent and reasonable or the comparisons could be misleading. The outward growth of the shear layer is not in itself an accurate measurement of mixing. Rather, it is the region in which gases from both streams are present that constitutes the "mixed" fluid. The area A_{mix} is thus used as the measure of mixing.

The mixing area for the vortex case above, M_t=4.0, M_j=2.84, 80% Helium 20% Nitrogen injection, 45 degree vanes, is plotted in Figure 29. Areas between several different contour pairs

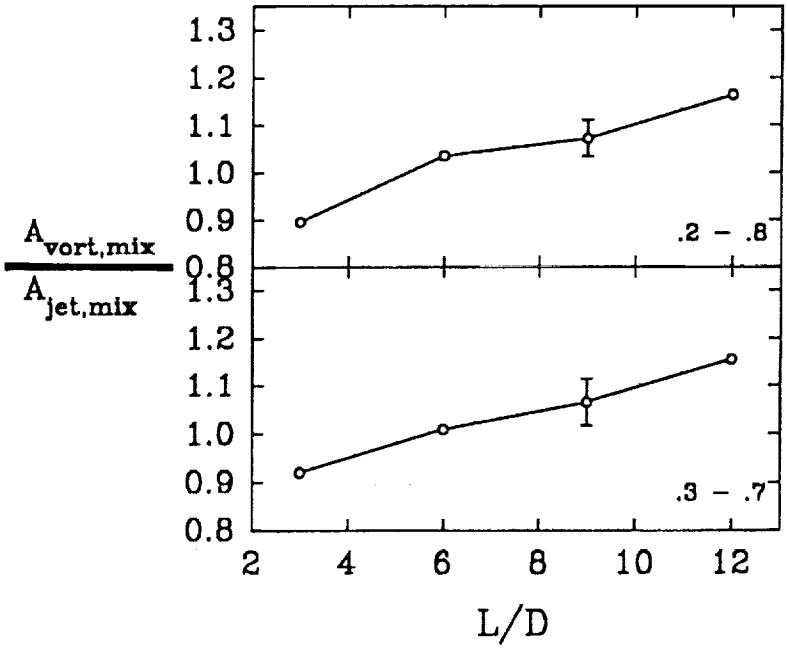

Figure 30 - Mixing area ratio (vortex/jet) as a function of L/D.

are shown. It appears as though any one of them may be representative of the mixing, however, the 0.3-0.7 and 0.2-0.8 contour pairs were chosen to present the results since the errors associated with these levels were the smallest.

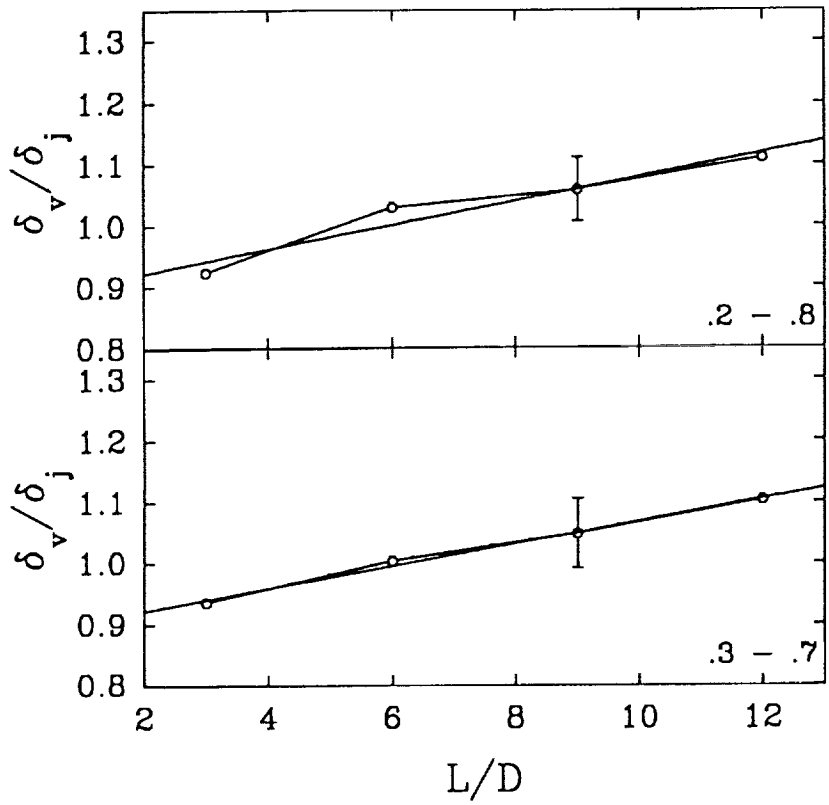

Figure 31 - shear layer thickness ratio (vortex/jet) as a function of L/D.

5.4.3 Mixing Area Ratios

To directly compare the vortex flow mixing characteristics with that of the jet, the ratio of vortex mixing area to jet mixing area ($A_{mix,v}/A_{mix,j}$) is calculated. This non-dimensionalization of the swirling flow by its non-swirling counterpart (the vanes are removed and all other parameters remain the same) is done to remove the effects of density ratio, velocity ratio, and compressibility in order to focus on the effect of swirl alone. The results for the same case as above, M_t=4.0, M_j=2.84, 80% Helium 20% Nitrogen injection, are plotted in Figure 30. It is obvious from either contour pair, 0.3-0.7, or 0.2-0.8, that the vortex mixing area is growing at a faster rate than the jet; this accounts for the positive slope of the line. Note that it appears as though the vortex mixing area has grown about 25% more than the jet mixing area over the first 12 diameters.

5.4.4 Shear Layer Thickness Ratio

Rather than comparing the slopes of $A_{mix,v}/A_{mix,j}$ versus L/D, the slope of the ratios of the shear layer thickness $delta_v/delta_j$ versus L/D are compared. This more traditional method of examining mixing layers has been used in the past (Papamoschou & Roshko[10](1988)) to compare compressible shear layers with their incompressible counterpart, having the same density and velocity ratios. The slope of these curves is an accurate measure of the relative increase or decrease of mixing so that different cases may be compared.

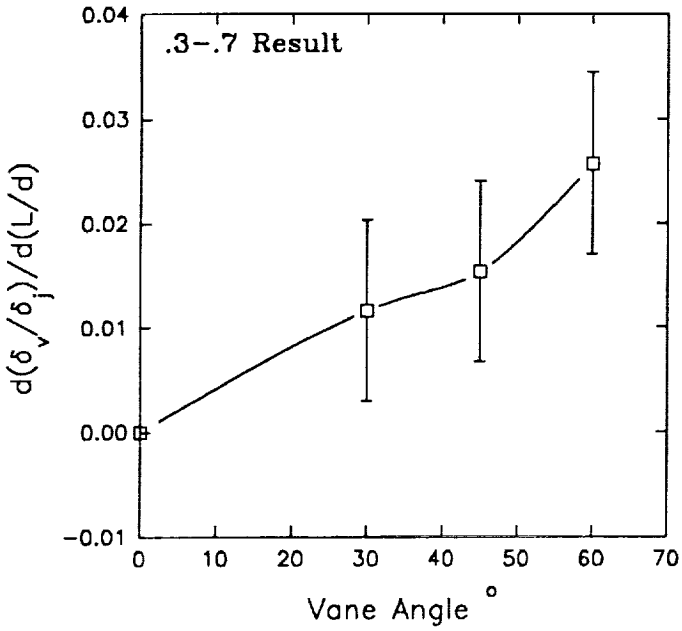

Figure 32 - Mixing enhancement parameter vs. Mach number

In order to plot the non-dimensionalized shear layer thickness, the equivalent axisymmetric shear layer thickness was calculated for each vortex, $delta_v$ and non-dimensionalized by the corresponding jet shear layer thickness, $delta_j$. This quantity was then plotted versus L/D as shown in Figure 31. As one would expect, Figure 30 and Figure 31 look very similar, as one would expect. Fitting a straight line to the points in Figure 32, and calculating the slope, $d(\delta_v/\delta_j)/d(L/D)$, yields a single value that represents the mixing layer growth enhancement due to the addition of swirl. Repeating this process for each vortex case in Table 4 yields the results in Table 5.

GAS	M	VANE ANGLE	M	LEVELS			
				.1-.9	.2-.8	.3-.7	.4-.6
He	3.0	30	1.3	.0002	.0073	**.0116**	.0124
He	3.0	45	1.3	.0033	.0096	**.0154**	.0153
He	3.0	60	1.3	.0106	.0190	**.0257**	.0263
He	3.7	45	1.6	-.0163	.0103	.0188	.0223
He	4.5	45	1.9	.0087	0.000	.0049	.0039
He-N	2.6	45	0.7	.0119	.0196	.0183	.0190

Table 5 - Image analysis results. Shaded values are plotted in figure 32.

5.4.5 Spreading Rate Increase Comparison

At this point, it is important to consider the differences among the several cases tested. The most significant difference is the amount of swirl for a given case. All the cases in Table 2 have

significantly different swirl. Therefore, if the swirl were known quantitatively, then all the cases could be plotted against swirl and the effectiveness of swirl in enhancing mixing would be revealed.

However, the problem with considering only swirl is that there are other parameters being varied as well. The velocity ratio, $R = u_t/u_i$, density ratio, $S = \rho_t/\rho_i$, and the convective Mach number, M_c are known to be accounted for in the non-dimensionalization of each case, but the effect of density ratio and convective Mach number on the vortex effectiveness in enhancing the mixing is not known. Does increasing M_c dampen the effect of the vorticity? Does the value of the density ratio enhance or dampen the effect of vorticity? Both convective Mach number and density ratio vary with the gases used, so these effects are not readily separable. However, if all the results are plotted versus swirl, and collapse to a given curve, then it may be assumed that density ratio and convective Mach number have no effect on the mixing enhancement due to swirl. If this were true, then the convective Mach number and density ratio only matter for the dimensional growth rate and are accounted for with the proper non-dimensionalization.

The swirl for all the cases above, as stated before, has yet to be calculated. However, for the 3 helium cases that only varied the swirl vanes, the vanes themselves may be used as a parameter to represent swirl. The mixing layer growth enhancement, $d(\delta_v/\delta_j)/d(L/D)$, is plotted versus vane angle in Figure 32 for the $M_t = 4.0$, $M_i = 2.95$ helium injection cases. The point at the origin is added since by definition, this curve must pass through zero. The obvious trend is that the greater the vane angle, the greater the mixing enhancement. The highest point on the curve, for the 60 degree vanes, represents 30% greater mixing area for the vortex, compared to the jet, at 12 L/D.

The error bars in Figure 32 represent an estimate of the error in the slope of the line in Figure 31. These error are not evaluated from the regression analysis, but rather are based on the errors associated with points used in the curve fit. Details of this calculation is given in Bowker and Lieberman[68](1972).

No results for the air injection cases are presented. This is due to the problems of visually evaluating the thickness of a low velocity ratio shear layer. Shear layers with little or no shear have been reported to be dominated by the initial boundary layer (Brown and Roshko[8](1974)). The shear layer must be investigated very far downstream for the wake-like flow to become a true mixing layer. In the present case, the initial boundary layer is known to be thick, Figure 15, and the near-field region is being investigated. Both of these factors suggest that the image data for those cases with low shear are most likely of to be of little value. Unfortunately, this also includes the one case of vortex breakdown examined thus far.

6. CONCLUSIONS AND FUTURE WORK

6.1 Conclusions

With the data obtained and reduced thus far, the following statements can be made: swirl enhances compressible mixing, the amount of mixing enhancement increases with increasing swirl, and the maximum increase in mixing area observed was about 30% at 12 L/D. The mechanism behind this mixing enhancement is still unknown. Also, the effect of convective Mach number and density ratio on the enhancement effect of swirl is also unknown.

6.2 Future Work

Some additional work is necessary to ensure that this study is complete. First, the swirl must be quantified such that the exact relationship between swirl and mixing enhancement may be understood. Secondly, instantaneous light sheet images must be reduced and compared to the time-averaged images already reduced. This is necessary to insure that the results from the time-averaged images are truly representative of mixing. In addition, further processing of these images may reveal information about the turbulence in the shear layer. Third, it must be shown that the particles being used to scatter the laser light follow the flow. Fourth, the spreading rates determined by the image analysis must be compared to those measured by other means in order to verify the technique. Finally, the mechanism behind the mixing enhancement has yet to be conclusively determined. Detailed approaches to each of these problems are presented below.

6.2.1 Swirl Quantification

6.2.1.2 Experimental Measurements

The reason that the swirl has not been measured to date is that the five-hole probe exceeded its limits in the highly swirling flowfields. In addition, the probe was only calibrated for air, so surveys in other gas combinations were not possible. Thus, another technique, LDV, will be employed to determine the swirl. Below, the steps that will be taken to determine the swirl are discussed.

First, a weak air vortex will be generated using the free-jet test stand. The resulting vortex will be measured with both LDV and five-hole probe to verify the LDV results. Once the proper operation of the system is verified, the Mach 2.9 helium vortex velocity profile will be measured with 3 sets of swirl vanes. Also, the M=2.84 He-N_2 vortex generated with the 45° vanes will be measured. These cases will also be investigated using the free-jet facility. Due to pressure limitations, the higher Mach number cases using helium will not be tested in the free jet. With these results, over a wide range of swirl and exit Mach number, empirical relationships for swirl will be

sought. With these relationships, the quantification of the vortex strength for each case will be possible. The methods of quantifying the vortices is discussed below.

6.2.1.2 Vortex Quantification Methods

Settles and Cattafesta[69] have considered methods of quantifying supersonic vortical flows. Several of these methods will be used to quantify the vortices strengths from the flowfield surveys. The result that appears to best reflect the physics of compressible swirling flow will be utilized to characterize the swirl for the cases listed in Table 4.

6.2.2 Instantaneous Image Reduction

The instantaneous PLS images of several of the cases in Table 4 will be reduced. An algorithm addressing particular problems associated with the reduction of these instantaneous images is in the process of being developed. The information contained in the instantaneous images can be analyzed in many ways. Several images can be averaged, and then reduced in a similar manner to the time-averaged images. However, from the instantaneous images, we know that large departures from the mean structure occur (Figure 4). Therefore, the question arises, whether the time averages represent the average mixing area, or are they simply a limit of the distance the structures stretch? This can be easily tested by reducing many instantaneous images separately and averaging the results.

In addition, turbulent-like quantities can be determined from these images. For instance, the average and fluctuating length of a given intensity-level contour may be calculated. Also, the average and fluctuating intensity of a given region may be calculated.

6.2.3 Particle Dynamics

It is important to insure that the particles are following the flow closely if the laser light sheet images are to be representative of mixing. The particle sizes have already been estimated; however, it remains to be seen whether these particles follow the flow.

The problem of flow tracking will be approached in two ways. One approach is to model the flowfield and predict the tracks of the particles. This is done by using the experimentally-measured velocity field, or some representation thereof, and assuming an equation of motion for the particle of a given mass and size. This equation is then solved by numerically integrating the equation of motion. Performing this integration for numerous time steps yields the particle position as a function of time. This position may be compared with a fluid particle path starting

from the same location.

The second approach is to use information in the literature concerning particle tracking. Any particle tracking models or experiments in vortical flow will be analyzed.

6.2.4 Verification Of Image Analysis Results

To verify whether or not the results from the image analysis are reasonable, comparison will be made with other results. A wide range of data exists within the literature against which the spreading rate of the pure jet cases may be compared. Although the resulting shear layer thicknesses may differ significantly depending on the method used to evaluate the shear layer thickness (Papamoschou and Roshko[10](1988)), the results should show the same tendencies.

6.2.5 Vortex Mixing Enhancement Mechanisms

From the results to date it appears as though the mixing enhancement may involve the modification of large scale structure. It has been noted by many researchers that these structures control turbulent mixing. In addition, many analytical studies have pointed out that azimuthal instability mechanisms are enhanced in swirling flows. Finally, from instantaneous images of the shear layer, the large scale structure of the vortical flow appears to be different from that of the jet flow.

Aside from the instantaneous images already taken, optical deflectometry experiments are being planned to study the turbulent structure of the shear layer. Figure 33 shows the schlieren-based optical deflectometer developed by McIntyre and Settles[25]. This instrument is sensitive to density fluctuations in the flow. Thus it yields a time record of the density gradient. Single-point measurements yield spectral information about the turbulence. Two-point measurements can be taken either on the same or opposite sides of the shear layer. Varying the distance between the two points on the same side of the shear layer yields information on the convective velocity and evolution of structures. Looking at the signal from opposite sides of the shear layer can yield information about the phase of the structures from which the helicity of the structures may be derived.

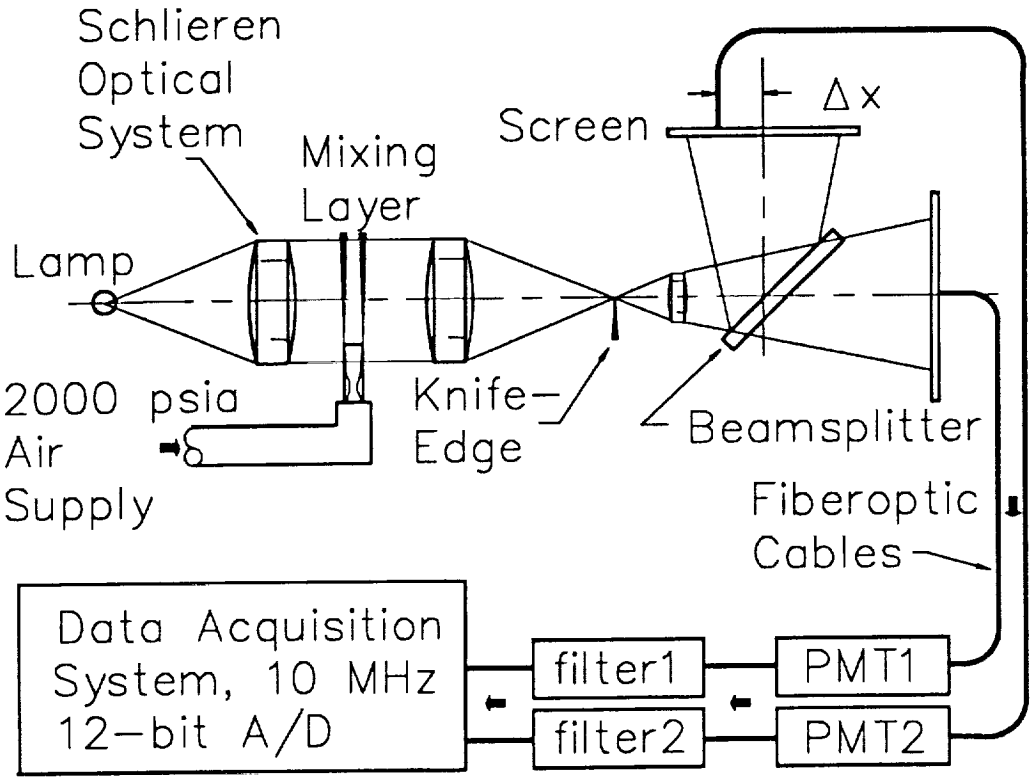

Figure 33 - Optical deflectometry setup. From McInyre and Settles[25].

REFERENCES

1. Northam, G.B., Anderson, G.Y., " Ramjet Research at Langley," AIAA-86-0159, 1986.

2. Northam, G.B., Greenberg I., Byington, C.S., " Evaluation of Parallel Injector Configurations for Supersonic Combustion," AIAA-89-2525, July 1989.

3. Drummond, J.P., Carpenter, M.H., Riggins, D.W., Adams, M.S., " Mixing Enhancement in a Supersonic Combustor," AIAA-89-2794, July, 1989.

4. Seiner, J.M., Kresja, E.A., " Supersonic Jet Noise and High Speed Civil Transport," AIAA-2358, July 1989.

5. Swithenbank, J., et. al., " Turbulent Mixing in Supersonic Combustion Systems," AIAA-89-0260, 1989.

6. Lessen, M., Singh, P.J., & Paillet, F., " The Stability of a Trailing Line Vortex. Part Inviscid Theory," *Journal of Fluid Mechanics*, Vol. 63, part 4, pp. 753-763, 1974.

7. Kumar, A, Bushnell, D., Hussani, M., " A Mixing Augmentation Technique for Hypervelocity Scramjets," AIAA-87-1882, June-July 1987.

8. Dimotakis, P.E., " Turbulent Free Shear Layer Mixing," AIAA-89-0262, 1972.

9. Brown, G.L., Roshko, A.R., " On Density Effects and Large Structure in Turbulent Mixing Layers," *Journal of Fluid Mechanics*, Vol. 64, No. 4, pp 775-781, 1974.

10. Bogdanoff, D.W., " Compressibility Effects in Turbulent Shear Layers," *AIAA Journal*, Vol. 21, No. 6, June, 1983.

11. Papamoschou, D., Roshko, A.R., " The Compressible Turbulent Shear Later: An Experimental Study," *Journal of Fluid Mechanics*, Vol. 197, pp 453-477, 1988.

12. Papamoschou, D., " Structure of the Compressible Turbulent Shear Layer," AIAA-89-0126, 1989.

13. Elliot, G., Samimy, M., " Compressibility Effects in Free Shear Layers," AIAA 90-0705, 1990.

14. Goebel, S.G., Dutton, J.C. " Velocity Measurements of Compressible, Turbulent Mixing Layers," AIAA-90-0709, 1990.

15. Elliot, G., Samimy, M., Reeder, M.F., " Pressure-Based Real-Time Measurements in Compressible Free Shear Layers," AIAA 90-1980, 1990.

16. Samimy, M., Erwin, D.E., Elliot, G.S., " Compressibility and Shock Wave Interaction Effects on Free Shear Layers," AIAA 89-2460, 1989.

17. Clemens, N.T., Mungal, M.G., Berger, T.E., Vandsburger, U., " Visualizations of the Structure of Turbulent Mixing Layer Under Compressible Conditions," AIAA 90-0500, 1990.

18. Clemens, N.T., Mungal, M.G., " Two- and Three-Dimensional Effects in the Supersonic Mixing Layer," AIAA-90-1978, July 1990.

19. Papamoschou, D., " Structure of the Compressible Turbulent Shear Layer," AIAA-89-0126, 1989.

20. Dolling, D.S., Fournier, E., Shau, Y.R., " The Effects of Vortex Generators on the Growth Rate of a Compressible Turbulent Shear Layer," AIAA-90-1979, July 1990.

21. Shau, Y.R., Dolling, D.S., " Experimental Study of Spreading Rate Enhancement of High Mach Number Turbulent Shear Layers," AIAA-89-2458, July 1989.

22. Clemens, N.T., Mungal, M.G. " Side-Wall Shock Vortex Generator for Supersonic Mixing Enhancement," submitted to *Journal of Propulsion and Power*, September, 1990.

23. Gutmark, E., Schadow, K.C., Wilson, K.J., " Mixing Enhancement in Coaxial Supersonic Jets," AIAA-89-1812, 1989.

24. Fourgette, D., Dibble, R., Mungal, M., " Time Evolution of the Shear Layer of a Supersonic Axisymmetric Jet at Matched Conditions," AIAA-90-0508, January, 1990.

25. McIntyre, S.S., Settles, G.S., " Optical Experiments on Axisymmetric Compressible Turbulent Mixing Layers," AIAA-91-0623, January 1991.

26. Fourgette, D.C., Mungal, M.G., Barlow, R.S., Dibble, R.W., " Concentration Measurements in a Supersonic Shear Layer," AIAA-91-0627, 1991.

27. Lepicovsky, J., Ahuja, K.K., Brown, W.H., Burrin, R.H., " Coherent Large-Scale Structure in High Reynolds Number Supersonic Jets," *AIAA Journal*, Vol. 25, No. 11, pp. 1419 - 1425, November 1987.

28. Samimy, M., Zaman, K., Reeder, M., " Supersonic Jet Mixing Enhancement by Vortex Generators", AIAA 91-2263, 1991.

29. Tam, C.K.W., Hu, F.Q., " On the Three Families of Instability Waves of High Speed Jets," *Journal of Fluid Mechanics*, Vol. 201, pp. 447-483, 1989.

30. Morris, P.J., Giridharan, M.G., Viswanathan, K., " Turbulent Mixing in Plane and Axisymmetric Shear Layers," AIAA-90-0708, 1990.

31. Escudier, M., " Confined Vortices in Flow Machinery," *Annual Review of Fluid Mechanics*, 1987, No. 19, pp. 27-52.

32 Chigier, N.A., Chervinsky, A., " Experimental Investigation of Swirling Vortex Motion in Jets," *Journal of Applied Mechanics*, Transactions of ASME, Ser E, 34, pp. 443-451, June 1967.

33. Delery, J., Horowitz, E., Leutcher, O., Solignac, J.L., " Fundamental Studies on Vortex Flows," *Recherche Aerospatiale*, 2, 1984.

34. Lessen, M., Singh, P.J., & Paillet, F., "The Stability of a Trailing Line Vortex. Part Inviscud Theory," *Journal of Fluid Mechanics*, Vol. 63, part 4, pp. 753-763, 1974.

35. Lessen, M., & Paillet, F., " The Stability of a Trailing Line Vortex. Part 2. Viscous Theory," *Journal of Fluid Mechanics*, Vol. 65, part 4, pp. 769-779, 1974.

36. Leibovich, S., & Stewartson, K., " A Sufficient Condition for the Instability of Columnar Vortices," *Journal of Fluid Mechanics*, Vol. 126, pp. 335-356, 1983.

37. Uberoi, M.S., Chow, C., & Narain, J.P., " Stability of Coaxial Rotating Jet and Vortex of Different Densities," *Physics of Fluids*, Vol. 15, No. 10, pp 1718-1727, 1972.

38. Povinelli, L.A., Ehlers, R.C., "Swirling Base Injection for Supersonic Combustion Ramjets," *AIAA Journal*, Vol. 10, No. 9, September 1972, pp. 1243-1244.

39. Schetz, J.A., Swanson, R.C., " Turbulent Jet Mixing at High Supersonic Speeds," *Z. Flugwiss.*, 21, 5, pp. 166-173, 1973.

40. Swithenbank, J., Chigier, N.A., " Vortex Mixing for Supersonic Combustion," XIIth International Symposium on Combustion, Poitiers, France, 1968. Mono of Maryland, Baltimore 1969, pp. 1152-1162.

41 Tillman, T.G., Patrick, W.P., Paterson, R.W., " Enhanced Mixing of Supersonic Jets," AIAA-88-3002, 1988.

42 Tillman, T.G., Paterson, R.W., Prescz, W.M. Jr., " Supersonic Nozzle Mixer Ejector," AIAA-89-2925, 1989.

43 Driscoll, R.J., " Mixing Enhancement in Chemical Lasers, Part 1:Experiments," *AIAA Journal*, Vol. 24, No. 7, July 1986, pp. 1120-1126.

44. Naughton, J., Cattafesta, L., Settles, G., " An Experimental Study of the Effect of Streamwise Vorticity on Supersonic Mixing Enhancement," AIAA-89-2456, 1989.

45. Khorrami, M.R., " Stability of Compressible Swirling Jet," AIAA-91-1770, 1991.

46. Hall, M.G., " Vortex Breakdown," *Annual Review of Fluid Mechanics*, Vol. 4, pp. 195-218, 1972.

47. Leibovich, S., " The Structure of Vortex Breakdown," *Annual Review of Fluid Mechanics*, Vol. 10, pp. 221-246, 1978.

48. Benjamin, T.B., " Theory of the Vortex Breakdown Phenomenon," *Journal of Fluid Mechanics*, Vol. 14, pp. 593-629, 1962.

49. Leibovich, S., & Randall, J.D., " Amplification and Decay of Long Nonlinear Waves," *Journal of Fluid Mechanics*, Vol. 53, part 3, pp. 481-493, 1973.

50. Faler, J.H. & Leibovich, S., " Disrupted States of Vortex Breakdown," *Physics of Fluids*, Vol. 20, No. 9, pp 1385-1400, 1977.

51. Metwally, O., " The Interaction Between a Supersonic Streamwise vortex and a Normal Shock Wave," PhD. dissertation, Penn State University, 1989.

52. Metwally, O., Settles, G., Horstmann, C., " An Experimental Study of Shock Wave/Vortex Interaction," AIAA-89-0082, 1989.

53. Cattafesta, L.N., Settles, G.S., " Experiments on Shock/Vortex Interaction," Extended Abstract submitted for presentation at the AIAA 30th Aerospace Sciences Meeting, Reno, NV, January 6-9, 1992.

54. Cutler, A.D., Levey, B.S., " Vortex Breakdown in a Supersonic Jet," AIAA-91-1815, 1991.

55. Naughton, J.W., Cattafesta, L.C., Settles, G.S., " A Miniature Fast-Response 5-Hole Probe for Supersonic Flowfield Measurements," Extended Abstract submitted for presentation at the AIAA 30th Aerospace Sciences Meeting, Reno, NV, January 6-9, 1992.

56. Kegelman, J., " A Flow-Visualization Technique for Examining Complex Three-Dimensional Flow Structures," Proc. 10th Symposium on Turbulence, University of Missouri-Rolla, September, 1986.

57. Clemens, N.T., Mungal, M.G., " A Planar Mie Scattering Technique for Visualizing Supersonic Mixing Flows," *Experiments in Fluids*, No. 11, pp 175-185, 1991.

58. Alvi, F.S., Settles, G.S., " A Physical Model of the Swept Shock/Boundary-Layer Flowfield," AIAA-91-1768, June 1991.

59 Samimy, M., Lele, S.K., " Particle laden Compressible Free Shear Layers," AIAA-90-1977, July 1990.

60. Maurice, M.S., " The Effect of Particle Dynamics on LV Measurement Bias in Compressible, Vortical Flows," AIAA-91-0292, January 1991.

61. Centolazi, F.J., " Characteristics of a 40° Cone for Measuring Mach Number, Total Pressure, and Flow Angles at Supersonic Speeds," NACA-TN-3967, May 1957.

62. Rosensweig, R.E., Hottel, H.C., Williams, G.C., " Smoke-Scattered Light Measurement of Turbulent Concentration Fluctuation," *Chemical Engineering Science*, Vol. 15, pp 111-129, 1961.

63. Schneiderman, A.M., Sutton, G.W., "Laser Planogram Measurements of Turbulent Mixing Statistics in the Near Wake of a Supersonic Cone," *Physics of Fluids*, Vol. 13, No. 7, July 1970, pp 1679-1682.

64. Chao, Y.C., Han, J.M., Jeng, M.S., "A Quantitative Laser Sheet Image Processing Method for the Study of the Coherent Structure of a Circular Jet Flow," *Experiments in Fluids*, No. 9, pp 323-332, 1990.

65. Gonzales, R.C., Wintz, P., *Digital Image Processing*, 2nd ed., Reading MA, Addison-Wesley, 1987

66. Schackoff, R.J., *Digital Image Processing and Computer Vision*, New York, John Wiley and Sons, 1989.

67. Deissler, R.G., Perlmutter, M., "Analysis of the Flow and Energy Separation in a Turbulent Vortex," *Journal of Heat and Mass Transfer*, Vol. 1, pp 173-191, 1960.

68. Bowker, A.H., Lieberman, G.J., *Engineering Statistics*, 2nd ed., Englewod Cliffs, NJ, Prentice-Hall, 1972.

69. Settles, G.S., Cattafesta, L.C., " Supersonic Shock Wave/Vortex Interaction," Interim Technical Report on NASA Grant NAG-2-575, September, 1991.

70. Sarpakaya, T., " Vortex Breakdown in Swirling Conical Flows," *AIAA Journal*, Vol. 9, No. 9, pp. 1792-1799, 1971.